frontiers | Frontiers in Earth Science

TYPE Original Research
PUBLISHED 12 January 2023
DOI 10.3389/feart.2022.1037727

OPEN ACCESS

EDITED BY
Stanislaw Mazur,
Institute of Geological Sciences, Polish Academy of Sciences, Poland

REVIEWED BY
Wang Fangyue,
Hefei University of Technology, China
Yi-Xiang Chen,
University of Science and Technology of China, China
Yongsheng He,
China University of Geosciences, China

*CORRESPONDENCE
Huawen Cao,
caohuawen1988@126.com

SPECIALTY SECTION
This article was submitted to Structural Geology and Tectonics, a section of the journal Frontiers in Earth Science

RECEIVED 06 September 2022
ACCEPTED 01 November 2022
PUBLISHED 12 January 2023

CITATION
Pei Q, Ma S, Li C, Liu F, Zhang Y, Xiao Y, Wang S, Wu J and Cao H (2023), *In-situ* boron isotope and chemical composition of tourmaline in the Gyirong pegmatite, southern Tibet: Implications for petrogenesis and magma source.
Front. Earth Sci. 10:1037727.
doi: 10.3389/feart.2022.1037727

In-situ boron isotope and chemical composition of tourmaline in the Gyirong pegmatite, southern Tibet: Implications for petrogenesis and magma source

Qiuming Pei[1], Shaobing Ma[1], Chenghong Li[1], Fei Liu[2], Yunhui Zhang[1], Yong Xiao[1], Shiming Wang[1], Jianfei Wu[3] and Huawen Cao[4]*

[1]Faculty of Geosciences and Environmental Engineering, Southwest Jiaotong University, Chengdu, China, [2]Institute of Mountain Hazards and Environment, Chinese Academy of Sciences, Chengdu, China, [3]Information Center, Ministry of Natural Resources of China, Beijing, China, [4]Chengdu Center, China Geological Survey, Chengdu, China

Leucogranitic rocks, mainly including leucogranite-pegmatite systems, have been found to be widely distributed in the South Tibetan Himalaya, and they have received considerable interest because of their significance in crustal evolution and associated rare-metal mineralization. Although the nature and geodynamic setting of the Himalayan leucogranites have been well documented by numerous studies, the pegmatites spatially associated with these leucogranites are still poorly understood. Tourmaline is a ubiquitous phase from the leucogranite to the pegmatite. We have therefore conducted *in situ* major and trace element and boron isotope investigations of tourmaline from the Gyirong pegmatite, synthesizing published data on the Gyirong leucogranite, to document the origin of tourmaline and its genetic implications. Two types of tourmaline (Tur-I & Tur-II) have been identified in this contribution and they are enriched in Fe, Si and Al but depleted in Mg and Ca, with Mg/(Mg+Fe) ratios ranging from 0.22 to 0.45. Accordingly, the tourmalines belong to the alkali group and have schorl composition. Trace elements, such as Zn, Ga, V, Sc, Li, Sn, Sr, and Co in the tourmalines are relatively enriched, whereas, other trace elements record low concentrations less than 10 ppm. The trace element concentrations of tourmaline are mainly controlled by melt composition. Morphological and geochemical characteristics reflect that the tourmalines from the Gyirong pegmatite are magmatic in origin. The Gyirong pegmatitic tourmalines have S-type granitoids and pegmatites boron isotopic signatures with a tight range of $\delta^{11}B$ values between –11.8 and –9.7‰, which is consistent with the magmatic tourmalines (Mg-poor) of the Gyirong leucogranite. This study suggests that the Gyirong pegmatite was the product of crustal anatexis and that the crustal metapelitic rocks within the Greater Himalayan Crystalline Complex were the most likely source components.

KEYWORDS
tourmaline, boron isotope, leucogranite, pegmatite, Tibet

1 Introduction

The India-Asia collision since the Early Cenozoic formed the largest Himalayan-Tibetan orogenic system on Earth (Yin and Harrison, 2000; Najman et al., 2010; Hu et al., 2016; Xu et al., 2017). Meanwhile, the ongoing continental collision-convergence processes triggered large-scale anatexis of the crust during the Late Eocene to Miocene and eventually generated the world's most famous voluminous leucogranite belt (Le Fort et al., 1987; Hou et al., 2012; Wu et al., 2015; Fan et al., 2021). As a probe, the Himalayan leucogranites carry ample information, such as their origin, age, emplacement mechanisms and related economic mineralization, which is critical for understanding the tectonic-magmatic-metamorphic evolution of the Himalayan orogeny (Searle et al., 2010; Liu et al., 2019; Wang et al., 2020; Wu et al., 2020; Tang et al., 2021; Xu et al., 2021; Cao H. et al., 2022). These leucogranitic rocks mainly include leucogranite-pegmatite systems, which are widely distributed in the South Tibetan Himalaya (Zhou et al., 2019). Considerable attention has been paid to the nature and geodynamic setting of the Himalayan leucogranites (Cao et al., 2022a and reference therein), while the pegmatites spatially associated with these leucogranites are still poorly understood.

Tourmaline, as a ubiquitous cyclosilicate mineral in rocks of the Earth's crust, forms in a wide range of geological settings and is particularly prevalent in evolved granitic rocks (Trumbull et al., 2008; van Hinsberg et al., 2011; Wadoski et al., 2011; Čopjaková et al., 2021). The chemical compositions of tourmaline have negligible diffusion rates with wide temperature (150 °C–900 °C) and pressure (6 MPa to >6 GPa) stability ranges, making it an ideal petrogenetic indicator (Henry et al., 2011; Wei and Zhao, 2020). Importantly, tourmaline is the dominant boron-bearing mineral, and its boron isotopes show significant variations. Therefore, tourmaline boron isotope geochemistry has been widely applied to trace boron sources and magmatic-hydrothermal processes (Marschall and Jiang, 2011; Grew et al., 2016; Guo et al., 2021; Guo et al., 2022). In addition, tourmaline occurs widely in Himalayan leucogranites and associated pegmatites, and often has well-defined crystal faces with complex zonal structures (Yang et al., 2015; Zhou et al., 2019; Liu et al., 2022; Zhang et al., 2022). Such convoluted chemical zoning retains the history of physicochemical conditions of the melt or fluid from which it crystallized and provides major insights into petrologic processes (Hawthorne and Dirlam, 2011; Bosi, 2018; Liu and Jiang, 2021).

The Gyirong aera, located in the central Himalayan orogenic belt, contains the vital record of sedimentary sequence, drainage development and magmatic-tectonic events of the Himalaya (Shen et al., 2016; Dong et al., 2017). Previous studies mainly focused on climatic and tectonic uplift evolution (Hong et al., 2010; Shen et al., 2016; Wolff et al., 2022), paleoenvironmental analysis (Xu et al., 2012), gneiss dome and associated granitoids (Gao and Zeng, 2014; Dong et al., 2017; Gao et al., 2017; Wang et al., 2017) and potential rare metal mineralization (Wu et al., 2020). The geochemical variations in accessory minerals such as zircon, monazite, tourmaline and garnet from the leucogranites are also involved in the above investigations (Gao et al., 2017; Hu et al., 2022), whereas there is a lack of studies on tourmaline from the pegmatites therein. In this contribution, we present *in situ* major and trace elements and boron isotopes of tourmalines from the Gyirong pegmatite of southern Tibet. Our results, combined with the geochemical data of the tourmalines from other regions along the Himalayan leucogranite belt, allow us to document the geochemical behavior of tourmaline precipitation and its origin, and also contribute additional constraints on the genetic mechanisms of the Himalayan leucogranites as well as the architecture and evolution of the Himalayan orogen.

2 Geological setting and samples

The roughly east-west-trending Himalayan orogen (extending ~2500 km long), bounded by the Indus-Yarlung Tsangpo suture to the north and the Main Front Thrust (MFT) to the south, is a classic example of collisional belts worldwide (Figure 1A) (Hodges, 2000; Zhao Z-b et al., 2021; Yu et al., 2021; Pan et al., 2022). It has experienced a prolonged and complicated history that included several periods of oceanic spreading, subduction and continental collision and eventually formed *via* the amalgamation of multiple terranes (Pan et al., 2012; Metcalfe, 2021; Xu et al., 2022). Tectonically, from north to south, four major lithotectonic units have been defined within this orogen: the Tethyan Himalayan Sequence (THS), the Greater Himalayan Crystalline Complex (GHC), the Lesser Himalayan Sequence (LHS) and the sub-Himalayan Sequence (SHS, or defined as the Siwalik Sequence), which are separated sequentially by the South Tibet Detachment System (STDS), the Main Central Thrust (MCT) and the Main Boundary Thrust (MBT) (Figure 1B) (Yin, 2006; Goscombe et al., 2018; Cao et al., 2020). The THS located in the northernmost part of the orogenic belt mainly exposed Early Paleozoic-Eocene clastic and carbonate rocks that experienced low-grade greenschist- and low amphibolite-facies metamorphism (Cao et al., 2018). A series of discontinuously distributed gneiss domes (e.g., the Malashan dome, Kawakami et al., 2007), belonging to the North Himalayan gneiss domes (NHGD) (Alsdorf et al., 1998; Fu et al., 2017; Ma et al., 2022), are recognized within the THS. The GHC consists of Proterozoic-Early Paleozoic high-grade metasediments, orthogneiss and magmatic rocks (Grujic et al., 2002; Gou et al., 2016; Gou et al., 2022; Ji et al., 2022),

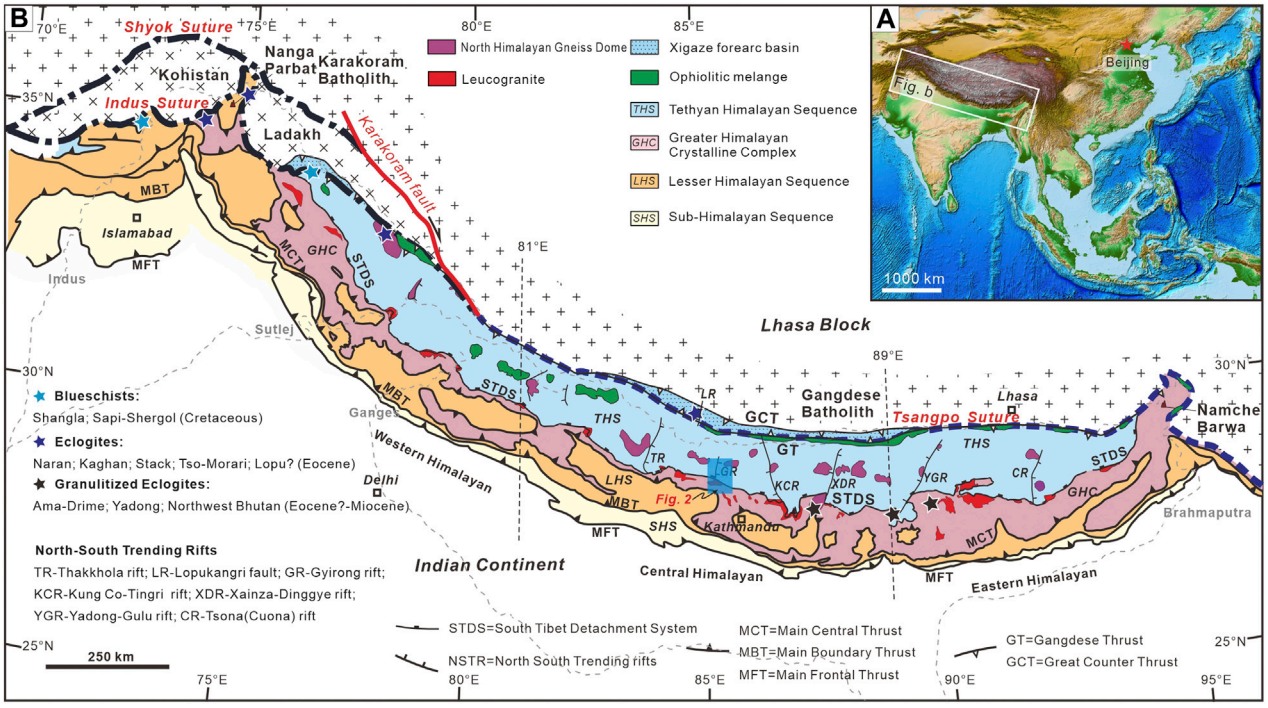

FIGURE 1
(A) Geographical location of the Himalaya. **(B)** Simplified geological map of the Himalayan Orogen (modified after Cao et al., 2021).

representing the core of the Himalayan orogenic belt. Further evidence suggests that it exhumed from the middle-lower crust to near the surface in the Cenozoic (Webb et al., 2017). The LHS principally comprises Paleoproterozoic to Early Paleozoic greenschist-to amphibolite-facies metasedimentary rocks, augen gneisses and metavolcanic rocks (Imayama et al., 2010; Martin, 2017). Two subparallel Cenozoic leucogranite belts with nearly east-west direction are discontinuously exposed along Himalayan orogen (Figure 1B): the northern belt occurs in the THS and NHGD, and the southern belt is distributed at the top of the GHC or involved in the shear zone beneath the STDS (Searle, 1999). Petrographically, the Himalayan leucogranites are generally equivalent to monzonite granites and dominated by two-mica (muscovite and biotite), biotite-, tourmaline- and garnet-bearing leucogranites (Wu et al., 2020). Their mineralogical composition includes quartz, euhedral plagioclase, perthitic potassic feldspar, muscovite, tourmaline, biotite and garnet (Guillot and Le Fort, 1995).

Our study area, which is located near the Gyirong County of southern Tibet, encompasses the Malashan-Paiku Co dome, the THS, the STDS, and the GHC from north to south (Figure 2). In addition, several Late Cenozoic fault basins, such as Gyirong and Oma, are also distributed in this area, which may be controlled by the north-south extension related to the STDS (Yang et al., 2009). The Malashan-Paiku Co dome acts as a segment of the NHGD and consists essentially of two-mica granite and Paiku composite leucogranite in the core and metamorphic rocks such as gneiss, schist and phyllite toward the margin (Wang et al., 2016; Gao et al., 2017), accompanied by multistage ductile deformation (Aoya et al., 2005). To the south, there is a set of Ordovician-Jurassic sedimentary rocks containing a small amount of Early Paleozoic and Mesozoic volcanic rocks. The cross-section of Gyirong area shows that folds and normal faults are developed in this set of strata. The STDS in the Gyirong area is a large ductile shear zone with a width of more than 10 km. It is mainly composed of Paleozoic granitic gneiss and Cenozoic foliated two-mica granites with syn-deformational features (Yang et al., 2009) and was emplaced by late undeformed leucogranites (~17.7 Ma, Gao et al., 2016). The GHC in the study area exposes medium-grade metamorphic rocks mainly consisting of augen gneiss, amphibole-biotite gneiss, metapelite, meta-sandstone, plagioclase-amphibole gneiss and schist. Leucogranites occurring as sills, dikes, dykes, dendritic and lenticular shapes intruded into the metamorphic rocks within the GHC. These leucogranitic veins were emplaced at 22–16 Ma (Wang et al., 2013; Gao et al., 2016), which record a long duration of anatexis and a tectonic transformation.

Two tourmaline-bearing samples (JL-4 and JL-5) were collected from the granitic pegmatites within the GHC (Figures 3A,B,D. Sample JL-4 is garnet tourmaline granitic

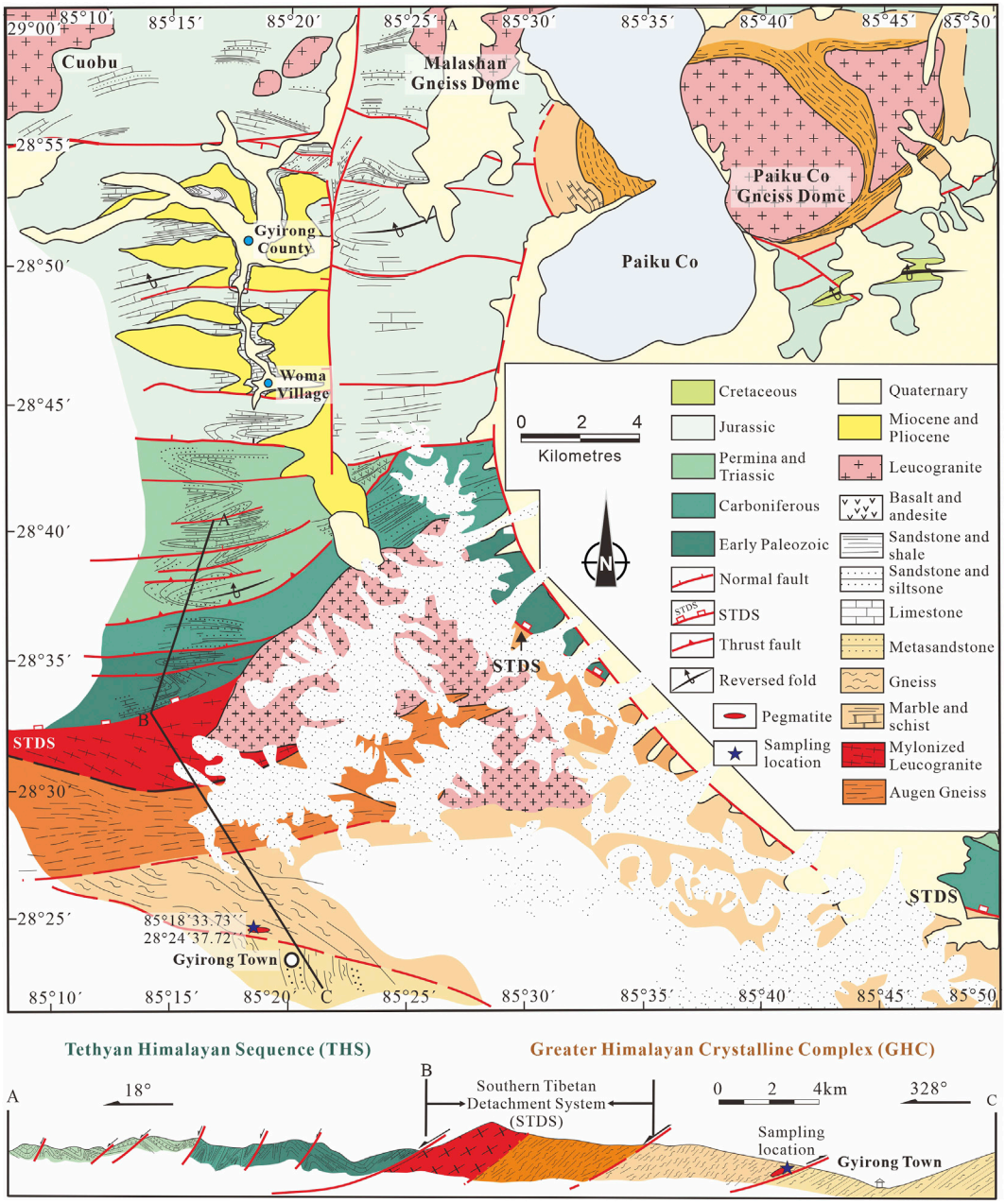

FIGURE 2
Geological map of the Malashan-Gyirong area (modified after Wang et al., 2017).

pegmatite. Plagioclase, potassium feldspar, tourmaline, garnet, muscovite and biotite dominate sample JL-4 (Figure 3C). Some tourmaline occurs as rounded inclusions within garnet (Figure 3C). In contrast, sample JL-5 displays similar mineral assemblages (Figures 3D–F) but much less garnet, thus it can be defined as tourmaline granitic pegmatite. Tourmaline in two samples shows diverse colors (e.g., green, brownish, yellow, pale blue) and usually has a dark- or light-colored core surrounded by a zoned rim. These tourmaline grains commonly occur as large crystals and are predominantly prismatic or granular in shape with sizes mainly ranging from 0.1 to 4 cm (Figures 3C,E–H). In this study, we select large tourmaline grains with complex zoning (Tur-Ⅰ type) within sample JL-4 and granular tourmaline (Tur-Ⅱ type) in sample JL-5 for further chemical and B isotope investigation.

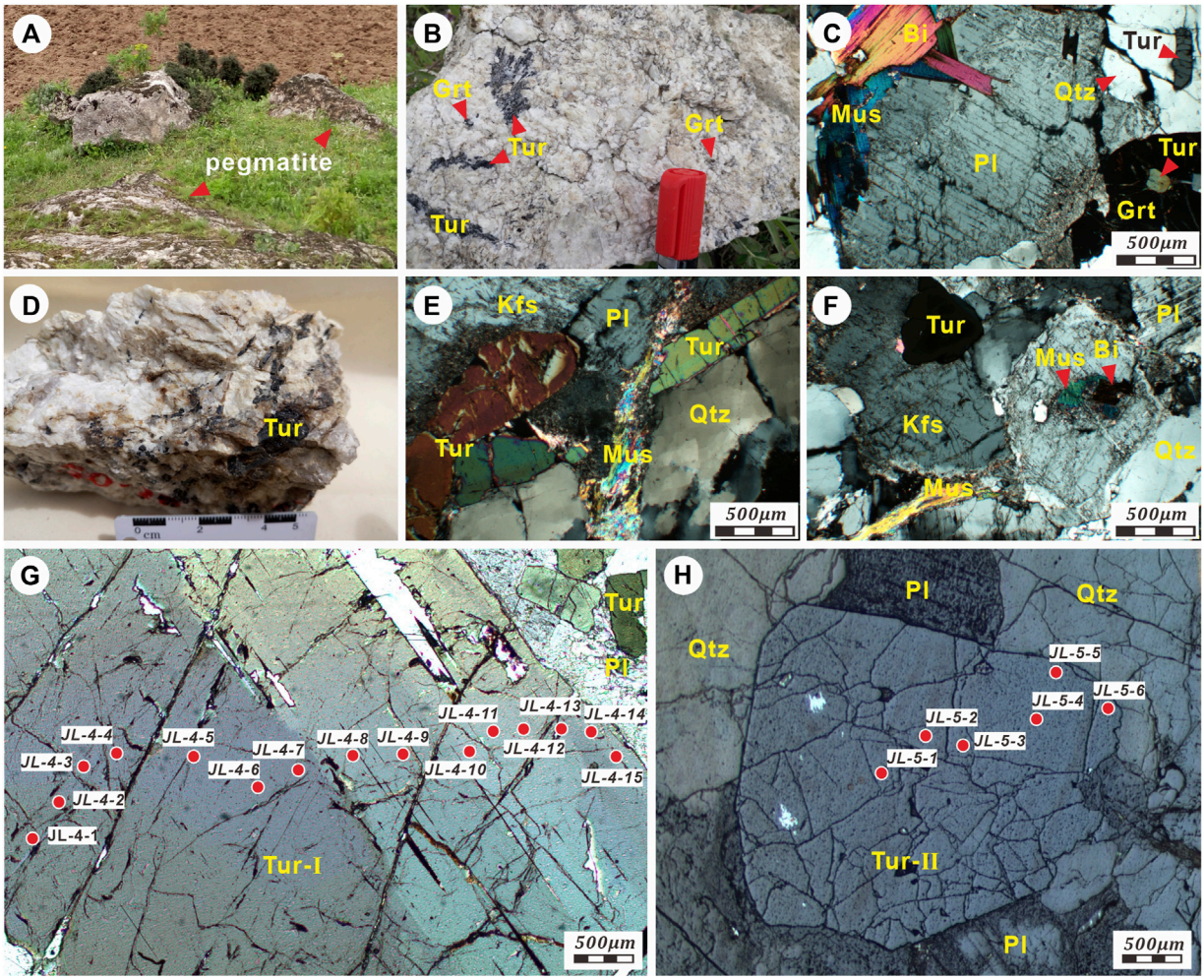

FIGURE 3
Representative photographs of tourmalines in the Gyirong pegmatite. **(A)** Outcrops of the Gyirong pegmatite. **(B)** Hand specimen of garnet tourmaline granitic pegmatite. **(C)** Granular tourmalines as rounded inclusions within garnet and quartz. **(D)** Hand specimen of tourmaline granitic pegmatite. **(E)** Large columnar tourmalines showing diverse colors. **(F)** Tourmaline grains, K-feldspar, plagioclase, quartz, muscovite and biotite in pegmatite. **(G)** Large tourmaline with complex zoning (Tur-I type). **(H)** Granular tourmaline (Tur-II type). The red circles are the points of *in situ*major and trace elements and boron isotope analyses. Abbreviations: Bi, Biotite; Grt, Garnet; Kfs, K-feldspar; Mus, Muscovite; Pl, Plagioclase; Qtz, Quartz; Tur, Tourmaline.

3 Analytical techniques

Major element compositions of tourmaline were obtained from polished thin sections using an EMPA-1600 electron microprobe with wavelength dispersive spectrometry at the Chengdu Center of the Geological Survey of China. The operating conditions were at 15 kV acceleration potential, 20 nA beam current and a 20 μm defocused spot with counting times between 10 and 30 s.

The trace element concentrations of tourmaline in polished thin sections were determined using an Agilent 7700E inductively coupled plasma mass spectrometer (ICP-MS) equipped to a GeolasPro laser ablation (LA) system at Wuhan Sample Solution Analytical Technology Co., Ltd., Wuhan, China. In this experiment, the ablating diameter for the LA-ICP-MS trace element analysis was set at 35 μm on the equivalent locations where the EPMA had been conducted. The detailed testing procedures and conditions were similar to those described by Zheng and Chen (2021). Data processing was performed offline using ICPMSDataCal software (Liu et al., 2008).

In situ boron isotopic compositions of tourmaline were measured in polished thin sections by the RESOlution S-155 laser ablation system coupled to a Nu plasma II multi-collector ICP-MS (LA-MC-ICP-MS). Analyses were carried out with laser spot size of 50 μm, 10 Hz repetition rate, and energy of ~5 J/cm^2. Two Faraday cups were used to collect $^{11}B/^{10}B$ signals of

TABLE 1 Summary of EPMA results and calculated atoms per formula (apfu) for tourmalines from the Gyirong pegmatites.

Sample	Tur-I-cores			Tur-I-rims			Tur-II		
	Min	Max	Mean	Min	Max	Mean	Min	Max	Mean
SiO_2	33.09	34.15	33.63	33.37	34.65	34.04	33.45	34.30	33.98
TiO_2	0.42	0.89	0.62	0.68	0.95	0.84	0.71	0.92	0.79
Al_2O_3	31.46	32.39	31.80	32.15	33.80	32.96	32.56	33.18	32.90
FeO	14.12	14.68	14.36	9.08	11.56	10.13	9.14	11.43	9.86
MnO	0.05	0.22	0.12	0.01	0.17	0.08	0.00	0.08	0.05
MgO	2.01	4.19	2.24	4.15	4.95	4.55	4.15	5.19	4.81
CaO	0.60	0.93	0.68	0.75	0.93	0.83	0.77	0.95	0.85
Na_2O	1.87	2.03	1.94	1.76	2.00	1.92	1.84	2.08	2.00
K_2O	0.07	0.11	0.09	0.07	0.10	0.08	0.06	0.10	0.07
B_2O_3	10.04	10.23	10.09	10.23	10.44	10.30	10.24	10.37	10.30
H_2O	3.28	3.36	3.30	3.32	3.40	3.37	3.33	3.42	3.37
O=F	0.00	0.00	0.00	0.00	0.03	0.00	0.00	0.06	0.02
Total(wt.%)	98.55	99.56	98.97	98.58	99.93	99.20	98.78	99.53	99.11
Structural formula on the basis of 15 Cations (T+Z+Y)									
B (apfu)	3.00	3.00	3.00	3.00	3.00	3.00	3.00	3.00	3.00
T site: Si	5.73	5.86	5.79	5.65	5.79	5.74	5.68	5.79	5.73
T site: Al	0.14	0.27	0.21	0.21	0.35	0.26	0.21	0.32	0.27
Z site: Al	6.00	6.00	6.00	6.00	6.00	6.00	6.00	6.00	6.00
Y site: Al	0.19	0.29	0.24	0.17	0.40	0.30	0.19	0.33	0.28
Y site: Fe^{2+}	2.03	2.12	2.07	1.26	1.64	1.43	1.29	1.62	1.39
Y site: Mg	0.52	1.06	0.58	1.05	1.23	1.14	1.05	1.31	1.21
X site: Ca	0.11	0.17	0.12	0.14	0.17	0.15	0.14	0.17	0.15
X site: Na	0.62	0.68	0.65	0.58	0.65	0.63	0.60	0.68	0.66
X site: K	0.02	0.03	0.02	0.01	0.02	0.02	0.01	0.02	0.02
X vacancy	0.18	0.24	0.21	0.18	0.25	0.20	0.14	0.22	0.17
V+W sites: OH	3.76	3.82	3.79	3.74	3.82	3.79	3.73	3.86	3.80
Mg/(Mg+Fe)	0.20	0.41	0.22	0.39	0.49	0.45	0.39	0.50	0.47

tourmaline samples and various standards. The standard-sample-standard bracketing (SSB) method was adopted to calibrate the instrumental mass fractionation (IMF). The international tourmaline standard IAEA B4 from Tonarini et al. (2003) served as an external standard, whereas tourmaline reference material IMR RB1 was adopted as the monitoring standard. Replicate analyses of standard tourmaline IMR RB1 yielded an average $\delta^{11}B$ of -13.3‰ (Supplementary Table S1), which is consistent with the reference value of −12.97‰ ± 0.97 (2σ; n = 57) obtained by LA-MC-ICP-MS (Hou et al., 2010). The external precision is estimated to be better than 0.5‰ (±2σ) based on the replicated analyses of reference tourmalines during the process of this study. The internal precision (1 SD) in per mil for individual analysis was calculated from approximately 100 cycles during each analysis (Zhao K-D. et al., 2021). Detailed analytical procedure broadly followed that presented in Yang and Jiang (2012).

4 Results

4.1 Tourmaline chemical compositions and classification

4.1.1 Major element crystal chemistry

Tourmaline has a fairly complicated crystal structure framework and varied constituents with empirical crystallochemical formula of XY_3Z_6 $[T_6O_{18}][BO_3]_3V_3W$ followed by (Hawthorne and Henry, 1999), where X = Na^+, Ca^{2+}, $X_{[vacancy]}$, K^+, Pb^{2+}; Y = Mg^{2+}, Fe^{2+}, Al^{3+}, Li^+, Ti^{4+}, Mn^{2+}, Fe^{3+}, Zn^{2+}; Z = Al^{3+}, Cr^{3+}, Fe^{3+}, Mg^{2+}, Fe^{2+}; T = Si^{4+}, B^{3+}, Al^{3+}; V = OH^-, O^{2-} ; and W = OH^- , F^- and O^{2-}. Tourmaline formulas were calculated by normalizing to 15 cations apfu (atoms per formula unit) in the tetrahedral and octahedral sites (T+Y+Z) and assuming B=3 pfu following the procedure of (Henry and Dutrow, 1996). The calculation was undertaken with the WinTcac program of Yavuz et al. (2014) based on the EPMA

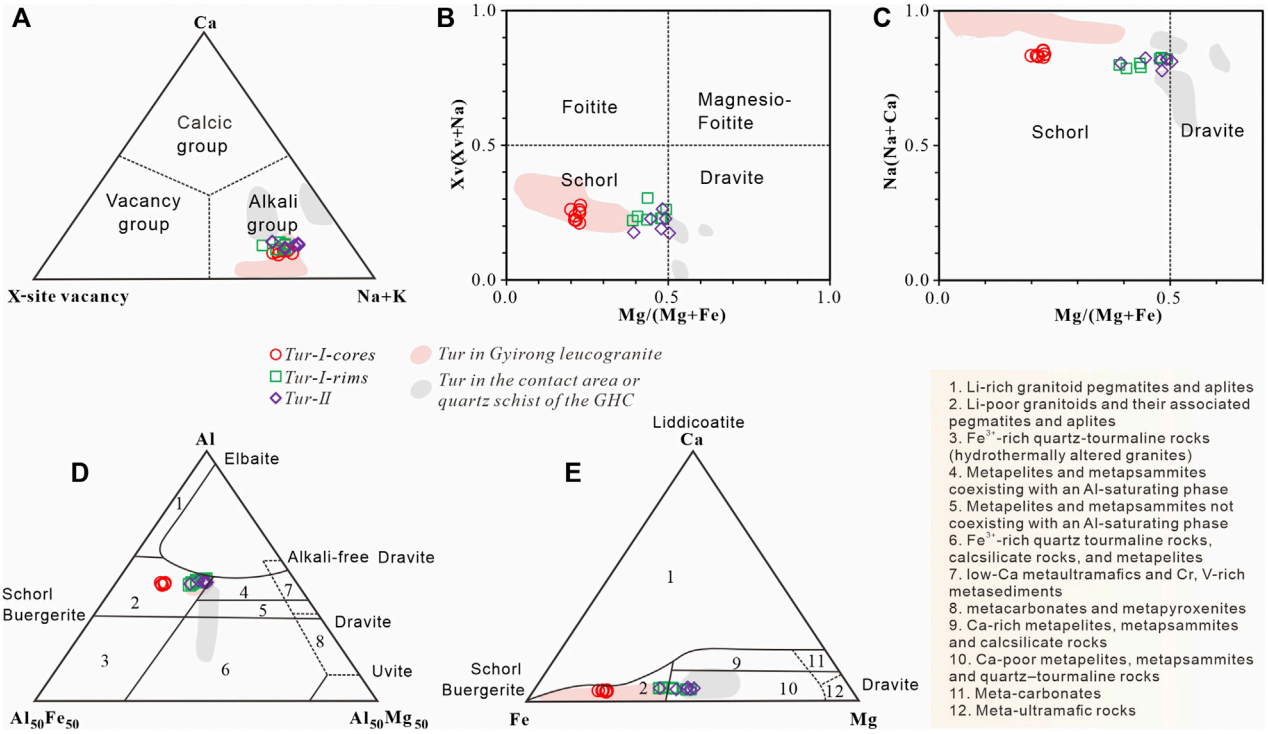

FIGURE 4
Ternary and binary diagrams for tourmaline in the Gyirong pegmatite. **(A)** Principal groups of tourmalines based on X-site occupancy (Henry et al., 2011). Plots of Mg/(Mg + Fe) vs. Xv/(Xv + Na) **(B)** and Mg/(Mg + Fe) vs. Na/(Na+Ca) **(C)** of tourmalines (Henry et al., 2011). **(D)** Ternary Al-Fe-Mg **(D)** and Ca-Fe-Mg **(E)** diagrams for tourmalines (Henry and Guidotti, 1985). Data sources: Hu et al.,(2018); Hu et al. (2022) and references therein.

data (Table 1). A complete list of the major element analyses can be found in Supplementary Table S2.

Tourmalines from the Gyirong pegmatite show large variable contents of FeO (9.08–4.68 wt.%) and MgO (2.01–0.19 wt.%) but restricted ranges of SiO_2 (33.09–34.65 wt.%), TiO_2 (0.42–0.95 wt.%), Al_2O_3 (31.46–3.80 wt.%), CaO (0.60–0.95 wt.%), Na_2O (1.76–0.08 wt.%) and K_2O (0.06–0.11 wt.%), with low K_2O (0.06–0.11 wt.%), MnO (0–0.22 wt.%) and F (0–0.06 wt.%). According to the X site classification of (Henry et al., 2011), all the tourmalines from the Gyirong pegmatite belong to the alkali group (Figure 4A). From the cores to the rims of Tur-I, a trend of lower FeO (14.68–0.13 wt.%) and higher MgO (2.24–0.55 wt.%) were found during crystal growth, whereas the concentrations of other major elements did not show clear differences. For tourmaline of Tur-II, its chemical composition is consistent with that of tourmaline rims of Tur-I. Thus, tourmalines from the Gyirong pegmatite are distributed in two groups: group-I of tourmaline cores of Tur-I, and group-II of tourmaline rims of Tur-I & tourmaline of Tur-II, with average $Mg^{\#}$ ($Mg^{\#}$=Mg/(Mg+Fe)) ratios of 0.22 and 0.45, respectively. The variations in the Y site $Mg^{\#}$ are shown in the plots of Mg/(Mg+Fe) versus the X-site occupancy (Xv/Xv+Na) (Figure 4B) and Mg/(Mg+Fe) v*ersus*the X-site occupancy (Na/Na+Ca) (Figure 4C). All the tourmaline samples exhibit small Na/Na+Ca and Xv/Xv+Na variations on the X-site, combined with $Mg^{\#}$ ratios, classifying them as schorl type (Figures 4B,C). As illustrated in Al-Fe-Mg and Ca-Fe-Mg ternary diagrams (Figures 4D,E) (Henry and Guidotti, 1985), tourmaline cores of Tur-I fall in field 2, equal to Li-poor granitoids and associated pegmatites and aplites. This is consistent with the negligible content of Li (less than 50 ppm) confirmed by the LA-ICP-MS analysis (see below). In contrast, some analyses of tourmalines from Tur-I rims and Tur-II fall in the range of Ca-poor metapelites, metapsammites and quartz-tourmaline rocks (field 10).

4.1.2 Trace element contents

The trace element compositions analyzed by LA-ICP-MS are summarized in Table 2, and the whole data set can be found in Supplementary Table S2. All types of tourmalines in the Gyirong pegmatite contain low contents of rare earth elements (REEs), with the majority of analyses yielding concentrations below 1 ppm. The total contents of REEs range from 13.3 to 23.9 ppm. Tourmalines of Tur-I and Tur-II from the Gyirong pegmatite share similar chondrite-normalized REE patterns

TABLE 2 Representative LA-ICP-MS trace element analyses of tourmaline from the Gyirong pegmatite (in ppm)

Sample	Tur-I-cores			Tur-I-rims			Tur-II		
	Min	Max	Mean	Min	Max	Mean	Min	Max	Mean
Li	21.13	44.95	33.49	17.27	21.95	19.37	16.05	21.36	18.54
Be	1.69	7.67	4.04	2.03	7.24	4.36	4.39	8.70	5.97
Sc	47.64	53.38	50.80	18.06	27.75	22.67	21.70	34.43	25.99
V	15.30	52.75	19.56	52.75	114.60	66.60	36.35	106.39	69.62
Co	9.49	16.64	10.51	16.64	19.29	18.17	15.12	19.75	17.77
Ni	0.12	6.53	1.51	6.53	13.63	10.80	3.02	18.52	9.75
Zn	299.74	333.63	315.98	195.69	228.70	212.44	207.77	259.31	224.08
Ga	79.92	94.54	84.88	83.99	97.23	90.08	89.17	97.50	93.34
Rb	0.02	0.10	0.05	0.02	0.12	0.07	0.02	0.15	0.09
Sr	15.71	26.43	17.47	20.11	26.43	22.86	17.08	25.49	20.64
Y	0.09	0.27	0.13	0.13	0.27	0.18	0.06	0.14	0.11
Sn	24.35	34.25	28.42	17.19	24.84	20.55	20.29	32.35	26.33
Sb	—	0.20	0.14	0.05	0.19	0.11	0.15	0.39	0.25
Pb	5.99	7.60	6.67	4.81	6.25	5.70	4.21	6.18	5.27
La	3.75	6.47	4.40	3.40	6.47	4.85	3.46	6.22	4.38
Ce	6.14	12.12	7.56	6.35	12.12	8.76	6.80	11.76	8.36
Pr	0.52	1.17	0.74	0.51	1.17	0.81	0.59	0.98	0.76
Nd	1.82	2.94	2.21	1.86	2.96	2.35	1.48	3.28	2.25
Sm	0.20	0.52	0.38	0.24	0.52	0.40	0.21	0.58	0.34
Eu	0.10	0.20	0.15	0.14	0.23	0.19	0.11	0.24	0.16
Gd	0.18	0.41	0.32	0.16	0.45	0.26	0.17	0.55	0.33
Tb	0.01	0.04	0.02	—	0.05	0.02	0.02	0.07	0.03
Dy	0.11	0.20	0.15	0.03	0.19	0.09	0.05	0.13	0.07
Ho	0.01	0.04	0.02	0.01	0.05	0.03	0.01	0.01	0.01
Er	0.02	0.04	0.04	0.04	0.07	0.05	0.03	0.06	0.05
Tm	0.02	0.02	0.02	0.01	0.04	0.02	0.02	0.02	0.02
Yb	0.01	0.16	0.06	0.08	0.16	0.11	0.06	0.12	0.09
Lu	0.01	0.03	0.02	0.01	0.02	0.02	0.03	0.03	0.03
ΣREE	13.7	23.9	16.0	13.3	23.9	17.8	13.7	23.2	16.8

"-" means below detection level.

(Figure 5), which are characterized by marked light REE enrichment with positive Eu anomalies and weak to negligible Ce anomalies. The concentrations of most trace elements except REEs vary from 0.1 to tens of parts per million (ppm) (Figure 6). Tourmalines are relatively enriched in Zn (195.56–333.63 ppm), Ga (79.92–7.50 ppm), V (15.30–14.60 ppm), Sc (18.06–3.38 ppm), Li (16.05–4.95 ppm), Sn (17.19–4.25 ppm), Sr (15.71–6.43 ppm) and Co (9.49–9.75 ppm). Whereas, trace elements such as Be, Ni, Rb, Y, Sb and Pb show concentrations less than 10 ppm. A few elements exhibit large variations in tourmaline of different types. Tourmalines in group-I display higher Li, Sc, Zn, Sn, and Pb contents than those in group-II. In contrast, elements such as V, Co, Ni and Sr are highly enriched in group-II.

4.2 Boron isotopic composition of tourmaline

The LA-MC-ICP-MS analytical results of boron isotopic compositions of tourmalines from the Gyirong pegmatite are available in Table 3 and Figure 7A. The tourmalines show a tight range of $\delta^{11}B$ values between -11.8 and -9.7‰. There seem to be no obvious differences in B-isotope compositions between the two types of tourmalines. More specifically, the $\delta^{11}B$ values of Tur-I from sample JL-4 and Tur-II from sample JL-5 are concentrated from −11.8 to −9.9‰ (mean −10.4‰) and from −11.8 to −9.7‰ (mean −11.1‰), respectively. With regard to compositional zonation, Tur-I shows slight core-rim variation, with mean $\delta^{11}B$ values ranging from −10.6‰ (core) to −10.2‰ (rim).

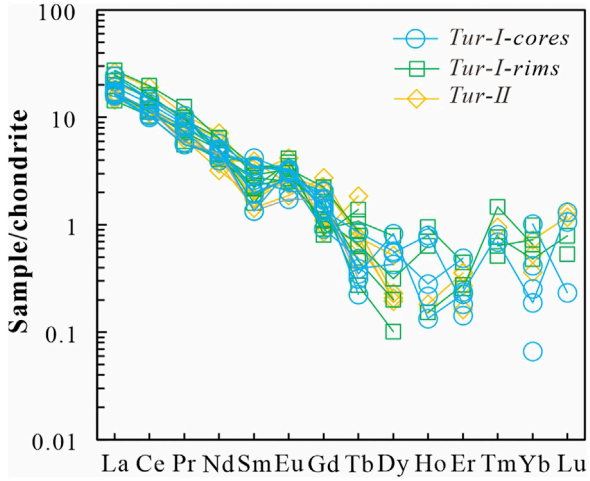

FIGURE 5
Chondrite-normalized REE diagrams of tourmalines in the Gyirong pegmatite.

5 Discussion

5.1 Formation of tourmaline in the Gyirong pegmatite

Tourmaline is a common accessory mineral in many evolved granitic rocks (Trumbull and Chaussidon, 1999; uriánek and Novák, 2007; Yang and Jiang, 2012), especially peraluminous leucogranites and related pegmatites, which widely exist in continental collision zones such as the Himalayan orogenic belt (Le Fort et al., 1987; Guillot and Le Fort, 1995; Wu et al., 2020; Liu et al., 2022). Abundant boron in melt-fluid system is the main factor for the crystallization of tourmaline (Wolf and London, 1997; London, 2011). Due to the incompatibility of boron and the crystallization of boron-poor materials (e.g., feldspar and quartz) during magma evolution, boron-rich magma may have been produced at late stage, causing tourmaline to crystallize (Pesquera et al., 2013). However, in the magmatic-hydrothermal stage, boron is preferentially partitioned into the fluid phase (London, 1999), and boron-rich fluid reacted with crystallized minerals and residual melts to form tourmaline nodules accordingly (Trumbull et al., 2008; Balen and Broska, 2011). Thus, tourmaline in the granite-pegmatite system could be magmatic in origin as documented by prior studies (Trumbull and Chaussidon, 1999; Chakraborty, 2021). Alternatively, it could also be generated from the reaction between boron-rich fluid with crystallized granite at shallow levels, as proven by field investigations and experimental works (Morgan and London, 1989; Cheng et al., 2019). Moreover, there are also examples of tourmaline in the pegmatite reported to be of magmatic-hydrothermal origin at the late magmatic stage (e.g., Gou et al., 2017). Accordingly, tourmaline in the pegmatite could potentially crystallize from a melt or (magmatic-) hydrothermal fluid, which requires comprehensive information to distinguish.

Tourmalines in the Gyirong pegmatite mainly act as isolated grains or long columnar coexisting with the major rock-forming minerals (quartz, plagioclase, K-feldspar, muscovite, etc.) with planar and arc-shaped contacts (Figures 3B,C,F–I). Furthermore, tourmaline crystals are found enveloped by quartz, feldspar and garnet grains (Figures 3B,C,F–I), suggesting that these tourmalines occurred early in the crystallization sequence. There is no textural evidence to show that pegmatite has undergone hydrothermal alteration. Geochemically, all the tourmaline samples reflect relatively homogeneous compositions and are characterized by low Mg# (0.20~0.50) and CaO (0.60–0.95 wt.%), high Al_2O_3 (31.46–3.80 wt.%) and FeO (9.08–4.68 wt.%), and high Al contents at the Y-site (0.19–40 apfu). All tourmalines belong to the alkali group (Figure 4A) and plot in the schorl (Fe-rich) field (Figures 4B,C). In the ternary diagrams of Al-$Al_{50}Fe_{50}$-$Al_{50}Mg_{50}$ (Figure 4D) and Ca-Fe-Mg (Figure 4E), tourmalines plot mostly in the magmatic range, whereas few analyses of Tur-I rims and Tur-II lie across field 2 (Li-poor granitoids and associated pegmatites and aplites) to field 10 (Ca-poor metapelites, metapsammites and quartz-tourmaline rocks). All tourmaline analyses from the Gyirong pegmatite display high Zn concentrations (195.56–33.63 ppm), which indicate that they were crystallized from hydrous borosilicate melts (Veksler and Thomas, 2002; Hazarika et al., 2017). The above morphology and geochemistry of the tourmaline in the Gyirong pegmatite indicate that they are magmatic in nature (London and Manning, 1995), which is clearly different in composition from tourmaline of hydrothermal origin (Yang et al., 2015; Zhao H-D. et al., 2021; Liu et al., 2022). These features are consistent with those of magmatic tourmaline reported in other Himalayan leucogranites (Yang et al., 2015; Dai et al., 2019; Zhou et al., 2019; Cheng et al., 2021; Liu et al., 2022).

It is noteworthy that the Tur-I rims and Tur-II show slightly Mg (Ca)-rich and Fe-poor signatures compared to the Tur-I cores. The common explanation for the significant increase in $Mg^{\#}$ from the core to rim of tourmaline is magma mixing and input of external (Mg-rich) fluid (Jiang et al., 2008; Cheng et al., 2021). However, there is no field evidence, such as the presence of secondary tourmaline veins. Besides, the uniform B-isotope compositions (Tur-I & Tur-II) also argue against magma mixing or the involvement of external fluids (Palmer and Swihart, 1996; Albert et al., 2018; Qiu et al., 2021). Alternatively, considering that the composition of magmatic tourmaline depends on the nature of the melt (Liu and Jiang, 2021), the insignificant variations (e.g., Fe, Mg, Ca) in core-rim compositions of tourmaline might suggest that slight assimilation and contamination by wall rocks have occurred (Liu and Jiang, 2021; Qiu et al., 2021). The high-grade metamorphosed rocks with high-Mg/low-Fe compositions in the GHC have the

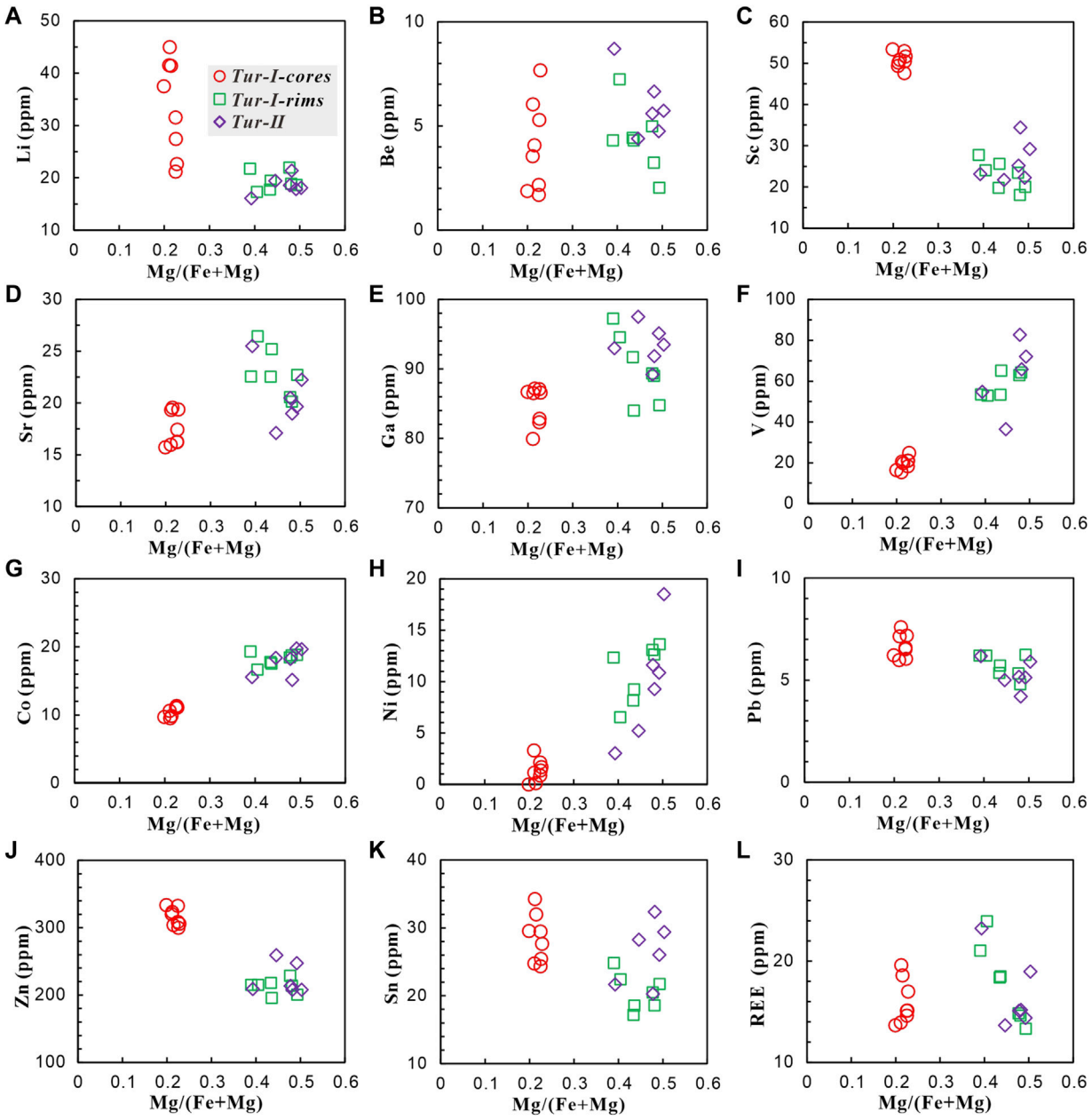

FIGURE 6
(A–L) Correlation diagrams between selected trace elements (Li, Be, Sc, Sr, Ga, V, Co, Ni, Pb, Zn, Sn, and REE) and Mg/(Mg + Fe) ratios in tourmalines from the Gyirong pegmatite.

potential to supply magnesium (Harris and Massey, 1994; Yin, 2006). The increase in V, Co and Ni and the decrease in Li with Mg/(Mg + Fe) from the Tur-Ⅰ cores to the Tur-Ⅰ rims and Tur-Ⅱ is consistent with contamination by the surrounding strata. This hypothesis is also supported by the distinct chemical variations in tourmalines in different lithologic units within the Gyirong area (Hu et al., 2022). Similarly, a transition trend recorded in elemental and Sr-Nd isotopic compositions of granitic dikes through Bendui intrusion to Himalayan leucogranites within the THS by a case study by Ji et al. (2020) also supports this scenario. It is worth noting that even if contamination by wall rocks might have occurred, the tourmaline composition only changes slightly (e.g., Mg# does not exceed 0.5). In this case, their boron isotopes can still represent the original B isotopic composition of the source (Hu et al., 2018).

TABLE 3 LA-MC-ICP-MS boron isotope analyses for tourmaline from the Gyirong granitic pegmatite

Analysis no.	Type	δ^{11}B (‰)	1 SD (‰)	Analysis no.	Type	δ^{11}B (‰)	1 SD (‰)
Sample JL-4							
JL-4-1	Tur-I	−11.6	0.9	JL-4-12	Tur-I	−9.9	0.7
JL-4-2	Tur-I	−11.3	0.8	JL-4-13	Tur-I	−9.9	0.8
JL-4-3	Tur-I	−11	0.8	JL-4-14	Tur-I	−9.9	0.7
JL-4-4	Tur-I	−11.8	0.8	JL-4-15	Tur-I	−9.9	0.7
JL-4-5	Tur-I	−10.6	0.9	Sample JL-5			
JL-4-6	Tur-I	−10.2	0.8	JL-5-1	Tur-II	−11	0.7
JL-4-7	Tur-I	−9.9	0.8	JL-5-2	Tur-II	−11.7	0.7
JL-4-8	Tur-I	−10	0.9	JL-5-3	Tur-II	−11.8	0.6
JL-4-9	Tur-I	−10.1	0.9	JL-5-4	Tur-II	−11.1	0.7
JL-4-10	Tur-I	−9.9	1	JL-5-5	Tur-II	−9.7	0.7
JL-4-11	Tur-I	−10	0.9	JL-5-6	Tur-II	−11	0.7

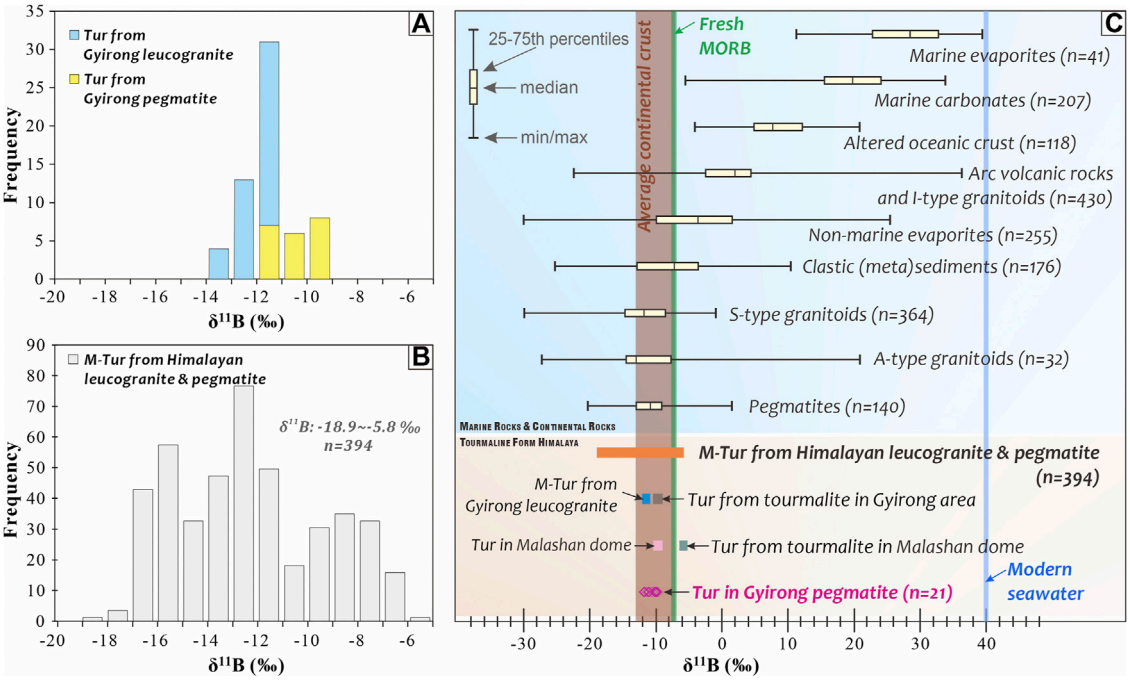

FIGURE 7
Histograms representing the δ^{11}B values of **(A)** tourmalines from the Gyirong leucogranite and pegmatite; and **(B)** magmatic tourmalines from Himalayan leucogranite and pegmatite. **(C)** Summary of boron isotope compositions for marine and crustal rocks and for tourmaline from the Gyirong and Malashan areas. Date sources: tourmalines from the Gyirong leucogranite (Hu et al., 2022), tourmalines from Himalayan leucogranites and pegmatites (Supplementary Table S3), average continental crust (Marschall and Jiang, 2011), and other boron reservoirs (Trumbull et al., 2020 and references therein). Abbreviations: Tur: tourmaline, M-Tur: magmatic tourmaline.

The trace elements of tourmaline could record the compositional signature of its host melt (e.g., van Hinsberg, 2011). According to the correlation diagrams of trace elements versus Mg/(Mg + Fe), only V, Ni and Co (not obvious) are positively correlated with Mg/(Mg + Fe) (Figure 6), which may be related to the potential crystal chemical effects on their incorporation (Zhao et al., 2019). Most trace elements did not show apparent correlations with

Mg/(Mg+Fe), which indicates that the trace element concentrations of tourmaline are mainly controlled by melt composition. This supports the scenario that tourmalines in the Gyirong pegmatite were crystallized directly from melt. In summary, we suggest that the tourmalines from the Gyirong pegmatite are of magmatic origin and are a product of direct crystallization from a boron-rich pegmatitic magma.

5.2 Boron isotope variation and genetic implications

We compiled a total of 394 boron isotopic analyses (Supplementary Table S3) on magmatic tourmalines (free of hydrothermal effects) from Himalayan leucogranites and pegmatites reported in the literature (Figure 7B, Chaussidon and Albarède, 1992; Yang et al., 2015; Gou et al., 2017; Hu et al., 2018; Dai et al., 2019; Zhou et al., 2019; Han et al., 2020; Cheng et al., 2021; Hu et al., 2022; Liu et al., 2022), which define an ample range of $\delta^{11}B$ values from −18.9 to −5.8. The large boron isotopic compositional variations in tourmalines in the Himalaya may result from heterogeneous melt sources (magma mixing) or fractions of boron isotopes during magma evolution (Trumbull et al., 2013; Kawakami et al., 2019; Xiang et al., 2020).

The measured tourmaline boron isotopes from the Gyirong pegmatite define a narrow range of −11.8 to −9.7 ‰ (concentrated at approximately −10 ‰) with negligible boron isotopic zonation within tourmalines, which indicates that no significant isotopic fractionation has occurred. Similarly, magmatic tourmalines (Mg-poor) of the Gyirong leucogranite have $\delta^{11}B$ values of −12.1 to −11.2 ‰ (Hu et al., 2022). Note that minimal boron isotope fractionation occurs between boric granitic or pegmatitic melt and tourmaline at common anatectic temperatures (Palmer and Swihart 1996; Smith and Yardley, 1996; Meyer et al., 2008). In this case, the boron isotopes of magmatic tourmaline should approximate that of the primary $\delta^{11}B$ value of the parental magma. The light boron isotopic compositions of magmatic tourmalines in the Gyirong leucogranite and pegmatite are consistent with the global database of average continental crust (−10 ± 3‰), S-type granitoids and pegmatites (Figure 7C), reflecting a continental source of boron (Trumbull et al., 2020).

As addressed by numerous studies (e.g., Gao and Zeng, 2014; Gou et al., 2017; Fan et al., 2021), the Himalayan leucogranites were mainly generated by metapelite dehydration melting or fluid-present melting. The Gyirong leucogranite shows high $(^{87}Sr/^{86}Sr)_i$ ratios (0.7548–7586), high Rb contents, and low Sr and Ba contents (Gao et al., 2017; Wang et al., 2017), which can be ascribed to fluid-absent melting of muscovite in metasedimentary sources. This interpretation is also supported by recent Mg-Fe-Sr-Nd isotope studies (e.g., Tian et al., 2020; Shi et al., 2021). Note that some authors found that the Himalayan leucogranites do not record any mantle material contribution to the sources (Inger and Harris, 1993; opkinson et al., 2017). In addition, some studies emphasized the contribution from the LHS fluids with regard to the anatectic sources of the Greater Himalayan leucagranites (Guo and Wilson, 2012; Liu et al., 2022). In contrast, there are also recent studies arguing that the contribution of the LHS is unnecessary (e.g., Ji et al., 2022). In our case, homogeneous tourmaline $\delta^{11}B$ values are consistent with the average crust and S-type granite, likely supporting the latter hypothesis in the Gyirong area. Hence, the crustal metapelitic rocks within the GHC were the most likely source components for the Gyirong pegmatite, which is consistent with most Himalayan leucogranites (Inger and Harris, 1993; Gao et al., 2017; Xie et al., 2018; Khanal et al., 2020; Hu et al., 2022; Ji et al., 2022).

Considering the close spatial and temporal relationship between the Gyirong leucogranite and pegmatite, it is easy to assume that the pegmatite originated from the highly differentiated evolution of granites. However, if this happened, the tourmaline in pegmatite could display lighter $\delta^{11}B$ values than that in leucogranite since the crystallization of tourmalines would result in depletion of ^{11}B in the residual melt (Chakraborty, 2021). As the melt cools, B-rich fluid exsolution from the magma often occurs in the granite-pegmatite systems (e.g., Thomas et al., 2003). Accordingly, tourmaline crystallized from the residual melt to show a lower $\delta^{11}B$ value (Liu et al., 2022). We have no conclusive evidence to confirm or deny the existence of hydrothermal tourmaline in the Gyirong pegmatite, which requires further investigation. In the present case, our measured boron isotope compositions of pegmatite ($\delta^{11}B$ of −11.8 to −9.7‰) show slightly higher values than those of the leucogranite ($\delta^{11}B$ of −12.1 to −11.2‰), which preclude the possibility of fractional crystallization (e.g., Rayleigh fractionation) as well as fluid exsolution (Ghosh et al., 2021). Such overlapping or similar B isotopic compositions in the granite-pegmatite system favor a genetic relationship between the Gyirong leucogranite and pegmatite (Montenegro et al., 2021). The Gyirong pegmatite displays high $^{87}Sr/^{86}Sr_{16Ma}$ (~0.762), $^{208}Pb/^{204}Pb_{16Ma}$ (~39.72), $^{207}Pb/^{204}Pb_{16Ma}$ (~15.79) and $^{206}Pb/^{204}Pb_{16Ma}$ (~19.6), and low εNd_{16Ma} value of −16.0 (authors' unpublished data). Their Sr-Nd-Pb isotopic signatures are consistent with those of the Gyirong leucogranite, suggesting that they have similar origins. Furthermore, the whole-rock geochemical data (authors' unpublished data) indicate that the Gyirong pegmatite did not experience a high degree of differentiation. Combined with the typical peraluminous mineral assemblage (e.g., tourmaline, muscovite and garnet) of the Gyirong pegmatite, we thus propose that the Gyirong pegmatite was the product of crustal anatexis rather than formed *via* the highly differentiated evolution of the granite. The anatectic metamorphism was linked to crustal thinning (28–5 a) caused by the STDS within the Himalayan orogen (Harris and Massey, 1994; Wang et al., 2017; Ding et al., 2021; Ji et al., 2022).

6 Conclusion

Based on petrographic and geochemical studies conducted on tourmaline from the Gyirong pegmatite within the South Tibet Himalaya, we reached the following conclusions.

1) Mineralogical characteristics show that Gyirong pegmatite belongs to the peraluminous S-type pegmatite and contains abundant tourmaline. Two types of tourmalines (Tur-Ⅰ & Tur-Ⅱ) were identified in this contribution and they are all Fe-rich schorl with low Mg# ratios (0.22 –.45). The trace element concentrations of tourmaline are mainly controlled by melt composition.
2) Morphological and geochemical characteristics indicate that the tourmalines from the Gyirong pegmatite are magmatic in origin. Insignificant variations in tourmaline boron isotopic composition from −11.8 to −9.7‰ indicate that the Gyirong pegmatite was derived from the continental crust. And the crustal metapelitic rocks within the GHC were the most likely source components for the Gyirong pegmatite.
3) We hypothesize that the Gyirong pegmatite was the product of crustal anatexis rather than formed *via*the highly differentiated evolution of the Gyirong leucogranite.

Data availability statement

The original contributions presented in the study are included in the article/supplementary material, further inquiries can be directed to the corresponding author.

Author contributions

QP and HC designed the project and helped to supervise this study. QP, FL, YZ, and YX conducted field investigations. QP, SM, and CL carried out EMPA and LA-ICP-MS analysis for major and trace element compositions. SM, CL, and SW are responsible for iin situboron isotope analysis. FL and JW assisted in data collection and analysis. All authors listed participated in the discussion and contributed to the writing of the manuscript.

Funding

This research received funding from the Second Tibetan Plateau Scientific Expedition and Research (SQ2019QZKK2203), the Key subject of Science and Technology Projects of Chinese Academy of Sciences (XDA19030303-02), the Sichuan Natural Science Foundation (2022NSFSC0410) and the National Natural Science Foundation of China (41802095).

Acknowledgments

We thank Kuidong Zhao for assistance in tourmaline boron isotope analysis. We also greatly appreciate the constructive comments and suggestions from the editor and three reviewers, which helped us considerably improve the paper.

Conflict of interest

The authors declare that the research was conducted in the absence of any commercial or financial relationships that could be construed as a potential conflict of interest.

Publisher's Note

All claims expressed in this article are solely those of the authors and do not necessarily represent those of their affiliated organizations, or those of the publisher, the editors and the reviewers. Any product that may be evaluated in this article, or claim that may be made by its manufacturer, is not guaranteed or endorsed by the publisher.

Supplementary material

The Supplementary Material for this article can be found online at: https://www.frontiersin.org/articles/10.3389/feart.2022.1037727/full#supplementary-material

References

Abert, C., Lana, C., Gerdes, A., Schannor, M., Narduzzi, F., and Queiroga, G. (2018). Archean magmatic-hydrothermal fluid evolution in the Quadrilátero Ferrífero (SE Brazil) documented by B isotopes (LA MC-ICPMS) in tourmaline. *Chemi. Geolo.* 481, 95–109. doi:10.1016/j.chemgeo.2018.02.002

Alsdorf, D., Brown, L., Nelson, K. D., Makovsky, Y., Klemperer, S., and Zhao, W. (1998). Crustal deformation of the Lhasa terrane, Tibet plateau from Project INDEPTH deep seismic reflection profiles. *Tectonics* 17 (4), 501–159. doi:10.1029/98tc01315

Aoya, M., Wallis, S. R., Terada, K., Lee, J., Kawakami, T., Wang, Y., et al. (2005). North-south extension in the Tibetan crust triggered by granite emplacement. *Geol.* 33 (11), 853–685. doi:10.1130/g21806.1

Balen, D., and Broska, I. (2011). Tourmaline nodules: Products of devolatilization within the final evolutionary stage of granitic melt? *Geolo. Soci. Londo. Speci. Publi.* 350 (1), 53–68. doi:10.1144/sp350.4

Bosi, F. (2018). Tourmaline crystal chemistry. *Ame. Mineralogist* 103 (2), 298–306. doi:10.2138/am-2018-6289

Buriánek, D., and Novák, M. (2007). Compositional evolution and substitutions in disseminated and nodular tourmaline from leucocratic granites: Examples from the Bohemian Massif, Czech Republic. *Lithos* 95 (1-2), 148–614. doi:10.1016/j.lithos.2006.07.006

Cao, H., Huang, Y., Li, G., Zhang, L., Wu, J., Dong, L., et al. (2018). Late Tiassic sedimentary records in the northern Tethyan Himalaya: Tectonic link with Greater India. *Geoscie. Fronti.* 9 (1), 273–921. doi:10.1016/j.gsf.2017.04.001

Cao, H. W., Li, G. M., Zhang, L. K., Dong, L., Gao, K., and Dai, Z. W. (2020). Monazite U-Th-Pb age of Liemai Eocene granites in the southern Tibet and its geological implications. *Sedimenta. Geolo. Tethyan Geolo.* 40, 31–42. doi:10.19826/j.cnki.1009-3850.(2020)02-0031-12

Cao, H-W., Li, G-M., Zhang, R-Q., Zhang, Y-H., Zhang, L-K., Dai, Z-W., et al. (2021). Genesis of the Cuonadong tin polymetallic deposit in the Tethyan Himalaya: Evidence from geology, geochronology, fluid inclusions and multiple isotopes. *Gondwana Rese.* 92, 72–101. doi:10.1016/j.gr.2020.12.020

Cao, H-W., Pei, Q-M., Santosh, M., Li, G-M., Zhang, L-K., Zhang, X-F., et al. (2022a). Himalayan leucogranites: A review of geochemical and isotopic characteristics, timing of formation, genesis and rare metal mineralization. *Earth-Science Revi.* 234, 104229. doi:10.1016/j.earscirev.2022.104229

Cao, H., Li, G., Zhang, L., Zhang, X., Yu, X., Chen, Y., et al. (2022b). Genesis of Himalayan leucogranite and its potentiality of rare-metal mineralization. *Sedimenta. Geolo. Tethyan Geolo.* 42 (2), 189–211. doi:10.19826/j.cnki.1009-3850.2022.04004

Chakraborty, T. (2021). Tourmaline growth and evolution in S-type granites and pegmatites: Constraints from textural, chemical and B-isotopic study from the Gingpur Shist Belt granitoids, eastern India. *Geol. Mag.* 158, 1657–1670. doi:10.1017/s0016756821000224

Chaussidon, M., and Albarède, F. (1992). Secular boron isotope variations in the continental crust: A ion microprobe study. *Earth Alaneta. Scie. Lette.* 108 (4), 229–421. doi:10.1016/0012-821x(92)90025-q

Cheng, L., Zhang, C., Yang, X., Qi, D., Zhou, Y., and Holtz, F. (2019). Experimental investigation of reactions between two-mica granite and boron-rich fluids: Implications for the formation of tourmaline granite. *Sci. China Earth Sci.* 62 (1674-7313), 1630–1644. doi:10.1007/s11430-019-9442-y

Cheng, L., Zhang, C., Liu, X., Yang, X., Zhou, Y., Horn, I., et al. (2021). Significant boron isotopic fractionation in the magmatic evolution of Himalayan leucogranite recorded in multiple generations of tourmaline. *Chemi. Geolo.* 571, 120194. doi:10.1016/j.chemgeo.2021.120194

Čopjaková, R., Prokop, J., Novák, M., Losos, Z., Gadas, P., Škoda, R., et al. (2021). Hydrothermal alteration of tourmaline from pegmatitic rocks enclosed in serpentinites: Multistage processes with distinct fluid sources. *Lithos* 308-381, 105823. doi:10.1016/j.lithos.2020.105823

Dai, Z., Li, G., Ding, J., Zhang, L., Cao, H., Zhang, Z., et al. (2019). Chemical and Boron Iiotopic Composition, and Significance of Tourmaline from the Conadong Tourmaline Granite, Tibet. *Earth Scie.* 44 (6), 1849–5189. doi:10.3799/dqkx.2019.043

Ding, H., Kohn, M. J., and Zhang, Z. (2021). Long-lived (ca. 22-24 Myr) partial melts in the eastern Himalaya: Petrochronologic constraints and tectonic implications. *Earth Alaneta. Scie. Lette.* 558, 116764. doi:10.1016/j.epsl.2021.116764

Dong, X., Liu, G., and Gou, Z. (2017). Cenozoic metamorphism and tectonic significance of the greater himalayan crystalline complex from the Gyirong area, southern Tibet. *Acta Petrolo. Sini.* 33 (8), 2342–5236.

Fan, J-J., Wang, Q., Li, J., Wei, G-J., Ma, J-L., Ma, L., et al. (2021). Boron and molybdenum isotopic fractionation during crustal anatexis: Constraints from the conadong leucogranites in the Himalayan Block, South Tibet. *Geochimica Geosmochimica Acta* 297, 120–412. doi:10.1016/j.gca.2021.01.005

Fu, J., Li, G., Wang, G., Huang, Y., Zhang, L., Dong, S., et al. (2017). First field identification of the conadong dome in southern Tibet: implications for EW extension of the North Himalayan gneiss dome. *Int. J. Earth Sci.* 106 (5), 1581–9156. doi:10.1007/s00531-016-1368-2

Gao, L-E., and Zeng, L. (2014). Fluxed melting of metapelite and the formation of Miocene high-CaO two-mica granites in the Malashan gneiss dome, southern Tibet. *Geochimica Geosmochimica Acta* 130, 136–515. doi:10.1016/j.gca.2014.01.003

Gao, L., Zeng, L., Wang, L., Hou, K., Gao, J., and Shang, Z. (2016). Timing of Different Crustal Partial Mmlting in the Himalayan Orogenic Belt and Its Tectonic Implications. *Acta Geolo. Sini.* 90 (11), 3039–5309.

Gao, L-E., Zeng, L., and Asimow, P. D. (2017). Contrasting geochemical signatures of fluid-absent versus fluid-fluxed melting of muscovite in metasedimentary sources: The Himalayan leucogranites. *Geology* 45 (1), 39–42. doi:10.1130/g38336.1

Ghosh, U., Upadhyay, D., Abhinay, K., and Mishra, B. (2021). Nature of the mineralizing fluids in the Balda and Motiya W-prospects, Western India: Constraints from chemical and B-isotope composition of tourmaline. *Chemi. Geolo.* 582, 120439. doi:10.1016/j.chemgeo.2021.120439

Goscombe, B., Gray, D., and Foster, D. A. (2018). Metamorphic response to collision in the Central Himalayan Orogen. *Gondwana Rese.* 57, 191–265. doi:10.1016/j.gr.2018.02.002

Gou, Z., Zhang, Z., Dong, X., Xiang, H., Ding, H., Tian, Z., et al. (2016). Petrogenesis and tectonic implications of the Yadong leucogranites, southern Himalaya. *Lithos* 256-257, 300–130. doi:10.1016/j.lithos.2016.04.009

Gou, G. N., Wang, Q., Wyman, D. A., Xia, X. P., Wei, G. J., and Guo, H. F. (2017). *In situ* boron isotopic analyses of tourmalines from Neogene magmatic rocks in the northern and southern margins of Tibet: Evidence for melting of continental crust and sediment recycling. *Solid Earth Scie.* 2 (2), 43–54. doi:10.1016/j.sesci.2017.03.003

Gou, Z. B., Liu, H., Li, J., Zhang, S. Z., Zhao, X. D., and Wang, S. W. (2022). Petrogenesis and geological implications of the Yadong Migmatites, South Tibet. *Sedimenta. Geolo. Tethyan Geolo.* 42, 279–287. doi:10.19826/j.cnki.1009-3850.2022.05008

Grew, E. S., Krivovichev, S. V., Hazen, R. M., and Hystad, G. (2016). Evolution of Structural Complexity in Boron Minerals. *Can. Mineral.* 54 (1), 125–413. doi:10.3749/canmin.1500072

Grujic, D., Hollister, L. S., and Parrish, R. R. (2002). Himalayan metamorphic sequence as an orogenic channel: insight from Bhutan. *Earth Plalaneta. Scie. Lette.* 198 (1), 177–911. doi:10.1016/s0012-821x(02)00482-x

Guillot, S., and Le Fort, P. (1995). Geochemical constraints on the bimodal origin of High Himalayan leucogranites. *Lithos* 35 (3), 221–324. doi:10.1016/0024-4937(94)00052-4

Guo, Z., and Wilson, M. (2012). The Himalayan leucogranites: Constraints on the nature of their crustal source region and geodynamic setting. *Gondwana Rese.* 22 (2), 360–736. doi:10.1016/j.gr.2011.07.027

Guo, R., Hu, X., Garzanti, E., and Lai, W. (2021). Boron isotope composition of detrital tourmaline: A new tool in provenance analysis. *Lithos* 400–401, 106360. doi:10.1016/j.lithos.2021.106360

Guo, J., Xiang, L., Zhang, R., Yang, T., Wu, K., and Sun, W. (2022). Chemical and boron isotopic variations of tourmaline deciphering magmatic-hydrothermal evolution at the Gejiu Sn-polymetallic district, South China. *Chemi. Geolo.* 593, 120698. doi:10.1016/j.chemgeo.2021.120698

Han, J., Hollings, P., Jourdan, F., Zeng, Y., and Chen, H. (2020). Inherited Eocene magmatic tourmaline captured by the Miocene Himalayan leucogranites. *Ame. Mineralogist* 105 (9), 1436–4140. doi:10.2138/am-2020-7608

Harris, N., and Massey, J. (1994). Decompression and anatexis of Himalayan metapelites. *Tectonics* 13 (6), 1537–4156. doi:10.1029/94tc01611

Hawthorne, F. C., and Dirlam, D. M. (2011). Tourmaline the indicator mineral: From atomic arrangement to viking navigation. *Elements* 7 (5), 307–132. doi:10.2113/gselements.7.5.307

Hawthorne, F. C., and Henry, D. J. (1999). Classification of the minerals of the tourmaline group. *Eur. J. Mineral.* 11, 201–216. doi:10.1127/ejm/11/2/0201

Hazarika, P., Upadhyay, D., and Pruseth, K. L. (2017). Episodic tourmaline growth and re-equilibration in mica pegmatite from the Bihar Mica Belt, India: Major-and trace-element variations under pegmatitic and hydrothermal conditions. *Geol. Mag.* 154 (1), 68–86. doi:10.1017/s0016756815000916

Henry, D. J., and Dutrow, B. L. (1996). Metamorphic tourmaline and its petrologic applications. *Revi. Mineralogy Geochemi.* 33 (1), 503–557.

Henry, D. J., and Guidotti, C. V. (1985). Tourmaline as a petrogenetic indicator mineral: A example from the staurolite-grade metapelites of NW Maine. *Ame. Mineralogist* 70 (1-2), 1–15.

Henry, D. J., Novak, M., Hawthorne, F. C., Ertl, A., Dutrow, B. L., Uher, P., et al. (2011). Nomenclature of the tourmaline-supergroup minerals. *Ame. Mineralogist* 96 (5-6), 895–913. doi:10.2138/am.2011.3636

Hodges, K. V. (2000). Tectonics of the Himalaya and southern Tibet from two perspectives. *Geol. Soc. Am. Bull.* 112 (3), 324–530. doi:10.1130/0016-7606(2000)112<324:tothas>2.0.co;2

Hong, H., Zhang, K., and Li, Z. (2010). Climatic and tectonic uplift evolution since ~7 Ma in Gyirong basin, southwestern Tibet plateau: cay mineral evidence. *Int. J. Earth Sci.* 99 (6), 1305–1135. doi:10.1007/s00531-009-0457-x

Hopkinson, T. N., Harris, N. B. W., Warren, C. J., Spencer, C. J., Roberts, N. M. W., Horstwood, M. S. A., et al. (2017). The identification and significance of pure sediment-derived granites. *Earth alaneta. Scie. Lette.* 467, 57–63. doi:10.1016/j.epsl.2017.03.018

Hou, K., Li, Y., Xiao, Y., Liu, F., and Tian, Y. (2010). *In situ* boron isotope measurements of natural geological materials by LA-MC-ICP-MS. *Chin. Sci. Bull.* 55 (29), 3305–1331. doi:10.1007/s11434-010-4064-9

Hou, Z-Q., Zheng, Y-C., Zeng, L-S., Gao, L-E., Huang, K-X., Li, W., et al. (2012). Eocene–Oligocene granitoids in southern Tibet: Constraints on crustal anatexis and tectonic evolution of the Himalayan orogen. *Earth Plalaneta. Scie. Lette.* 349-350, 38–52. doi:10.1016/j.epsl.2012.06.030

Hu, X., Garzanti, E., Wang, J., Huang, W., An, W., and Webb, A. (2016). The timing of India-Asia collision onset–Facts, theories, controversies. *Earth-Science Revi.* 160, 264–929. doi:10.1016/j.earscirev.2016.07.014

Hu, G., Zeng, L., Gao, L-E., Liu, Q., Chen, H., and Guo, Y. (2018). Diverse magma sources for the Himalayan leucogranites: Evidence from B-Sr-Nd isotopes. *Lithos* 314-315, 88–99. doi:10.1016/j.lithos.2018.05.022

Hu, G., Gao, L., Zeng, L., and Li, Y. (2022). Geochemical and Boron Isotopic Evidence that Tourmaline Records Country Rock Assimilation of Leucogranites in the Himalayan Orogen. *Acta Geolo. Sini.* 96 (1), 123–314. doi:10.1111/1755-6724.14800

Imayama, T., Takeshita, T., and Arita, K. (2010). Metamorphic P–T profile and P–T path discontinuity across the far-eastern Nepal Himalaya: investigation of channel flow models. *Jo.Metamorphi. Geolo.* 28 (5), 527–459. doi:10.1111/j.1525-1314.2010.00879.x

Inger, S., and Harris, N. (1993). Geochemical Constraints on Leucogranite Megmatism in the Langtang Valley, Nepal Himalaya. *Jo.Metrology* 34 (2), 345–638. doi:10.1093/petrology/34.2.345

Ji, W-Q., Wu, F-Y., Liu, X-C., Liu, Z-C., Zhang, C., Liu, T., et al. (2020). Pervasive Miocene melting of thickened crust from the Lhasa terrane to Himalaya, southern Tibet and its constraint on generation of Himalayan leucogranite. *Geochimica eosmochimica Acta* 278, 137–516. doi:10.1016/j.gca.2019.07.048

Ji, M., Gao, X-Y., and Zheng, Y-F. (2022). Geochemical evidence for partial melting of progressively varied crustal sources for leucogranites during the Oligocene–Miocene in the Himalayan orogen. *Chemi. Geolo.* 589, 120674. doi:10.1016/j.chemgeo.2021.120674

Jiang, S-Y., Radvanec, M., Nakamura, E., Palmer, M., Kobayashi, K., Zhao, H-X., et al. (2008). Chemical and boron isotopic variations of tourmaline in the Hnilec granite-related hydrothermal system, Slovakia: Constraints on magmatic and metamorphic fluid evolution. *Lithos* 106 (1–2), 1–11. doi:10.1016/j.lithos.2008.04.004

Kawakami, T., Aoya, M., Wallis, S. R., Lee, J., Terada, K., Wang, Y., et al. (2007). Contact metamorphism in the Malashan dome, North Himalayan gneiss domes, southern Tibet: a example of shallow extensional tectonics in the Tethys Himalaya. *Jo. Metamorphi. Geolo.* 25 (8), 831–583. doi:10.1111/j.1525-1314.2007.00731.x

Kawakami, T., Sakai, H., and Sato, K. (2019). Syn-metamorphic B-bearing fluid infiltrations deduced from tourmaline in the Main Central Thrust zone, eastern Nepal Himalayas. *Lithos* 348-349, 105175. doi:10.1016/j.lithos.2019.105175

Khanal, G. P., Wang, J-M., Wu, F-Y., Wang, J-G., and Yang, L. (2020). In-sequence buoyancy extrusion of the Himalayan Metamorphic Core, central Nepal: Constraints from monazite petrochronology and thermobarometry. *Jo.Asian Earth Scie.* 199, 104406. doi:10.1016/j.jseaes.2020.104406

Le Fort, P., Cuney, M., Deniel, C., France-Lanord, C., Sheppard, S. M. F., Upreti, B. N., et al. (1987). Crustal generation of the Himalayan leucogranites. *Tectonophysics* 134 (1), 39–57. doi:10.1016/0040-1951(87)90248-4

Liu, T., and Jiang, S-Y. (2021). Multiple generations of tourmaline from Yushishanxi leucogranite in South Qilian of Western China record a complex formation history from B-rich melt to hydrothermal fluid. *Ame. Mineralogist* 106 (6), 994–1008. doi:10.2138/am-2021-7473

Liu, Y., Hu, Z., Gao, S., Günther, D., Xu, J., Gao, C., et al. (2008). *In situ* analysis of major and trace elements of anhydrous minerals by LA-ICP-MS without applying an internal standard. *Chemi. Geolo.* 257 (1–2), 34–43. doi:10.1016/j.chemgeo.2008.08.004

Liu, Z-C., Wu, F-Y., Liu, X-C., Wang, J-G., Yin, R., Qiu, Z-L., et al. (2019). Mineralogical evidence for fractionation processes in the Himalayan leucogranites of the Ramba Dome, southern Tibet. *Lithos* 340, 71–86. doi:10.1016/j.lithos.2019.05.004

Liu, S., Zhang, G., Zhang, L., Liu, Z., and Xu, J. (2022). Boron isotopes of tourmalines from the central Himalaya: Implications for fluid activity and anatexis in the Himalayan orogen. *Chemi. Geolo.* 596, 120800. doi:10.1016/j.chemgeo.2022.120800

London, D., and Manning, D. A. C. (1995). Chemical variation and significance of tourmaline from Southwest England. *Econo. Geolo.* 90 (3), 495–519. doi:10.2113/gsecongeo.90.3.495

London, D. (1999). Stability of tourmaline in pei aluminous granite systems: Te boron cycle from anatexis to hydrothermal aureoles. *Eur. J. Mineral.* 11 (2), 253–622. doi:10.1127/ejm/11/2/0253

London, D. (2011). Experimental synthesis and stability of tourmaline: a historical overview. *Tana. Mineralogist* 49 (1), 117–316. doi:10.3749/canmin.49.1.117

Ma, Z. N., Han, Z. P., Li, Y. L., Bi, W. J., Xu, T. K., and Xiao, S. Q. (2022). Exhumation history of the Kampa dome in the southern Tibet: Evidence from low temperature thermochronology. *Sedimenta. Geolo. Tethyan Geolo.* 42, 300–309. doi:10.19826/j.cnki.1009-3850.2022.04009

Marschall, H. R., and Jiang, S-Y. (2011). Tourmaline Isotopes: No Element Lift Behind. *Elements* 7 (5), 313–931. doi:10.2113/gselements.7.5.313

Martin, A. J. (2017). A review of Himalayan stratigraphy, magmatism, and structure. *Gondwana Rese.* 49, 42–80. doi:10.1016/j.gr.2017.04.031

Metcalfe, I. (2021). Multiple Tethyan ocean basins and orogenic belts in Asia. *Gondwana Rese.* 100, 87–130. doi:10.1016/j.gr.2021.01.012

Meyer, C., Wunder, B., Meixner, A., Romer, R., and Heinrich, W. (2008). Boron-isotope fractionation between tourmaline and fluid: a experimental re-investigation. *Contrib. Mineral. Petrol.* 156 (2), 259–627. doi:10.1007/s00410-008-0285-1

Montenegro, T., Wul, J., de Luchi, M. L., Ribacki, E., and Trumbull, R. B. (2021). Chemical and boron isotope composition of tourmaline from pegmatites and their host rocks, Sierra de San Luis, Argentina. *Tana. Mineralogist* 59 (3), 467–944. doi:10.3749/canmin.2000072

Morgan, G. B., and London, D. (1989). Experimental reactions of amphibolite with boron-bearing aqueous fluids at 200 MPa: implications for tourmaline stability and partial melting in mafic rocks. *Contrib. Mineral. Petrol.* 102 (3), 281–927. doi:10.1007/bf00373721

Najman, Y., Appel, E., Boudagher-Fadel, M., Bown, P., Carter, A., Garzanti, E., et al. (2010). Timing of India-Asia collision: Geological, biostratigraphic, and palaeomagnetic constraints. *J. Geophys. Res.* 115 (B12), B12416. doi:10.1029/2010jb007673

Palmer, M. R., and Swihart, G. H. (1996). Boron isotope geochemistry; an overview. *ReviMineralogy aeochemi.* 33 (1), 709–474.

Pan, G., Wang, L., Li, R., Yuan, S., Ji, W., Yin, F., et al. (2012). Tectonic evolution of the Qinghai-Tibet Plateau. *Jo. of Asian Earth Scie.* 53, 3–14. doi:10.1016/j.jseaes.2011.12.018

Pan, G. T., Wang, L. Q., Yin, F. G., Geng, Q. R., Li, G. M., and Zhu, D. C. (2022). Researches on geological tectonic evolution of Tibetan Plateau: A review, recent advances, and directions in the future. *Sedimenta. Geolo. Tethyan Geolo.* 42, 151–175. doi:10.19826/j.cnki.1009-3850.2022.05004

Pesquera, A., Torres-Ruiz, J., García-Casco, A., and Gil-Crespo, P. P. (2013). Evaluating the Controls on Tourmaline Formation in Ganitic Systems: a Ccse Study on Paraluminous Granites from the Central Iierian Zzne (CIZ), Western Spain. *Jo. Metrology* 54 (3), 609–364. doi:10.1093/petrology/egs080

Qiu, K-F., Yu, H-C., Hetherington, C., Huang, Y-Q., Yang, T., and Deng, J. (2021). Tourmaline composition and boron isotope signature as a tracer of magmatic-hydrothermal processes. *Ame. Mineralogist* 106 (7), 1033–4104. doi:10.2138/am-2021-7495

Searle, M., Cottle, J., Streule, M., and Waters, D. (2010). Crustal melt granites and migmatites along the Himalaya: mMlt source, segregation, transport and granite emplacement mechanisms. *Earth anvironm. Scie. Transa. ofo. Soci. odinbu.* 100 (1-2), 219–323. doi:10.1017/s175569100901617x

Searle, M. P. (1999). Emplacement of Himalayan leucogranites by magma injection along giant sill complexes: examples from the Co Ou, Gachung King and Everest leucogranites (Nepal Himalaya). *Jo.Asian Earth Scie.* 17 (5), 773–873. doi:10.1016/s1367-9120(99)00020-6

Shen, T., Wang, G., Leloup, P. H., van der Beek, P., Bernet, M., Cao, K., et al. (2016). Controls on Cenozoic exhumation of the Tethyan Himalaya from fission-track thermochronology and detrital zircon U-Pb geochronology in the Gyirong basin area, southern Tibet. *Tectonics* 35 (7), 1713–3174. doi:10.1002/2016tc004149

Shi, Q., He, Y., Zhao, Z., Liu, D., Harris, N., and Zhu, D-C. (2021). Petrogenesis of Himalayan Lucogranites: Perspective From a Combined Elemental and Fe-Sr-Nd Isotope Study. *JGR. Solid Earth* 126 (8), e2021JB021839. doi:10.1029/2021jb021839

Smith, M. P., and Yardley, B. W. D. (1996). The boron isotopic composition of tourmaline as a guide to fluid processes in the southwestern England orefield: An ion microprobe study. *Geochimica Geosmochimica Acta* 60 (8), 1415–2147. doi:10.1016/0016-7037(96)00007-5

Tang, J-X., Yang, H-H., Song, Y., Wang, L-Q., Liu, Z-B., Li, B-L., et al. (2021). The copper polymetallic deposits and resource potential in the Tibet Plateau. *China Geolo.* 4 (1), 1–16. doi:10.31035/cg2021016

Thomas, R., Förster, H-J., and Heinrich, W. (2003). The behaviour of boron in a peraluminous granite-pegmatite system and associated hydrothermal solutions: a melt and fluid-inclusion study. *Contrib. Mineral. Petrol.* 144 (4), 457–472. doi:10.1007/s00410-002-0410-5

Tian, S., Hou, Z., Chen, X., Tian, H., Gong, Y., Yang, Z., et al. (2020). Magnesium isotopic behaviors between metamorphic rocks and their associated leucogranites, and implications for Himalayan orogenesis. *Gondwana Rese.* 87, 23–40. doi:10.1016/j.gr.2020.06.006

Tonarini, S., Pennisi, M., Adorni-Braccesi, A., Dini, A., Ferrara, G., Gonfiantini, R., et al. (2003). Intercomparison of Boron Iiotope and Concentration Measurements. Part I: Selection, Preparation and Homogeneity Tests of the

Iltercomparison Materials. *Geostand. Geoanal. Res.* 27 (1), 21–39. doi:10.1111/j.1751-908x.2003.tb00710.x

Trumbull, R. B., and Chaussidon, M. (1999). Chemical and boron isotopic composition of magmatic and hydrothermal tourmalines from the Sinceni granite–pegmatite system in Swaziland. *Chemi. Geolo.* 153 (1–4), 125–317. doi:10.1016/s0009-2541(98)00155-7

Trumbull, R., Krienitz, M-S., Gottesmann, B., and Wiedenbeck, M. (2008). Chemical and boron-isotope variations in tourmalines from an S-type granite and its source rocks: Te Eaongo granite and tourmalinites in the Dimara Belt, Namibia. *Contrib. Mineral. Petrol.* 155 (1), 1–18. doi:10.1007/s00410-007-0227-3

Trumbull, R. B., Beurlen, H., Wiedenbeck, M., and Soares, D. R. (2013). The diversity of B-isotope variations in tourmaline from rare-element pegmatites in the Borborema Province of Brazil. *Chemi. Geolo.* 352, 47–62. doi:10.1016/j.chemgeo.2013.05.021

Trumbull, R. B., Codeço, M. S., Jiang, S-Y., Palmer, M. R., and Slack, J. F. (2020). Boron isotope variations in tourmaline from hydrothermal ore deposits: a review of controlling factors and insights for mineralizing systems. *Ore Geolo. Revi.* 125, 103682. doi:10.1016/j.oregeorev.2020.103682

van Hinsberg, V. J., Henry, D. J., and Marschall, H. R. (2011). Tourmaline: a ideal indicator of its host environment. *Tana. Mineralogist* 49 (1), 1–16. doi:10.3749/canmin.49.1.1

van Hinsberg, V. J. (2011). Preliminary experimental data on trace-element partitioning between tourmaline and silicate melt. *Tana. Mineralogist* 49 (1), 153–613. doi:10.3749/canmin.49.1.153

Veksler, I. V., and Thomas, R. (2002). An experimental study of B-P- and F-rich synthetic granite pegmatite at 0.1 and 0.2 GPa. *Contrib. Mineral. Petrol.* 143 (6), 673–863. doi:10.1007/s00410-002-0368-3

Wadoski, E. R., Grew, E. S., and Yates, M. G. (2011). Compositional evolution of tourmaline-supergroup minerals from granitic pegmatites in the Larsemann Hills, East Antarctica. *Tana. Mineralogist* 49 (1), 381–405. doi:10.3749/canmin.49.1.381

Wang, X., Zhang, J., Liu, J., Yan, S., and Wang, J. (2013). Middle-Miocene transformation of tectonic regime in the Himalayan orogen. *Chin. Sci. Bull.* 58 (1), 108–117. doi:10.1007/s11434-012-5414-6

Wang, X., Zhang, J., and Wang, J. (2016). Geochronology and Formation Mechanism of the Paiku Granite in the Northern Himalaya, and is Tectonic implications. *Earth Scie.* 41 (6), 982–998. doi:10.3799/dqkx.2016.082

Wang, X., Zhang, J., and Yang, X. (2017). Geochemical Characteristics of the Leucogranites from Gyirong, South Tibet: Formation Mechanism and Tectonic Implications. *Geotectonica et Metallogenia* 41 (2), 354–638. doi:10.16539/j.ddgzyckx.2017.02.011

Wang, Z-Z., Liu, S-A., Liu, Z-C., Zheng, Y-C., and Wu, F-Y. (2020). Extreme Mg and Zn isotope fractionation recorded in the Himalayan leucogranites. *Geochimica eosmochimica Acta* 278, 305–231. doi:10.1016/j.gca.2019.09.026

Webb, A. A. G., Guo, H., Clift, P. D., Husson, L., Müller, T., Costantino, D., et al. (2017). The Himalaya in 3D: Slab dynamics controlled mountain building and monsoon intensification. *Lithosphere* 9 (4), L636.1–51. doi:10.1130/l636.1

Wei, S-D., and Zhao, J-H. (2020). Neoproterozoic tourmaline-bearing peraluminous granitoids in the Western Jiangnan Orogen, South China: Geochemistry, petrogenesis and tectonic implications. *Precambrian Rese.* 347, 105831. doi:10.1016/j.precamres.2020.105831

Wolf, M. B., and London, D. (1997). Boron in granitic magmas: sability of tourmaline in equilibrium with biotite and cordierite. *Contributions tineralogy metrology* 130 (1), 12–30. doi:10.1007/s004100050346

Wolff, R., Hölzer, K., Hetzel, R., Xu, Q., Dunkl, I., Anczkiewicz, A. A., et al. (2022). Spatially focused erosion in the High Himalaya and the geometry of the Main Himalayan Thrust in Central Nepal (85°E) from thermo-kinematic modeling of thermochronological data in the Gyirong region (southern China). *Tectonophysics* 834, 229378. doi:10.1016/j.tecto.2022.229378

Wu, F., Liu, Z., Liu, X., and Ji, W. (2015). Himalayan leucogranite: Petrogenesis and implications to orogenesis and plateau uplift. *Acta Petrolo. Sini.* 31 (1), 1–36.

Wu, F-Y., Liu, X-C., Liu, Z-C., Wang, R-C., Xie, L., Wang, J-M., et al. (2020). Highly fractionated Himalayan leucogranites and associated rare-metal mineralization. *Lithos* 352-353, 105319. doi:10.1016/j.lithos.2019.105319

Xiang, L., Romer, R. L., Glodny, J., Trumbull, R. B., and Wang, R. (2020). Li and B isotopic fractionation at the magmatic-hydrothermal transition of highly evolved granites. *Lithos* 376-377, 105753. doi:10.1016/j.lithos.2020.105753

Xie, J., Qiu, H., Bai, X., Zhang, W., Wang, Q., and Xia, X. (2018). Geochronological and geochemical constraints on the Cuonadong leucogranite, eastern Himalaya. *Acta Geochimi.* 37 (3), 347–539. doi:10.1007/s11631-018-0273-8

Xu, Y-D., Zhang, K-X., Wang, G-C., Jiang, S-S., Chen, F-N., Xiang, S-Y., et al. (2012). Extended stratigraphy, palynology and depositional environments record the initiation of the Himalayan Gyirong Basin (Neogene China). *Jo. osian Earth Scie.* 44, 77–93. doi:10.1016/j.jseaes.2011.04.007

Xu, B., Griffin, W. L., Xiong, Q., Hou, Z. Q., O'Reilly, S. Y., Guo, Z., et al. (2017). Ultrapotassic rocks and xenoliths from South Tibet: Contrasting styles of interaction between lithospheric mantle and asthenosphere during continental collision. *Geology* 45 (1), 51–45. doi:10.1130/g38466.1

Xu, B., Hou, Z. Q., Griffin, W. L., Zheng, Y. C., Wang, T., Guo, Z., et al. (2021). Cenozoic lithospheric architecture and metallogenesis in Southeastern Tibet. *Earth-Science Revi.* 214, 103472. doi:10.1016/j.earscirev.2020.103472

Xu, B., Hou, Z. Q., Griffin, W. L., O'Reilly, S. Y., Long, T., Zhao, Y., et al. (2022). Apatite halogens and Sr–O and zircon Hf–O isotopes: recycled volatiles in Jurassic porphyry ore systems in southern Tibet. *Chemi. Geolo.* 605, 120924. doi:10.1016/j.chemgeo.2022.120924

Yang, S-Y., and Jiang, S-Y. (2012). Chemical and boron isotopic composition of tourmaline in the Xiangshan volcanic–intrusive complex, Southeast China: Evidence for boron mobilization and infiltration during magmatic–hydrothermal processes. *Chemi. Geolo.* 312-313 (0), 177–819. doi:10.1016/j.chemgeo.2012.04.026

Yang, X., Zhang, J., Qi, G., Wang, D., Guo, L., Li, P., et al. (2009). Structure and deformation around the Gyirong basin, north Himalaya, and onset of the south Tibetan detachment system. *Sci. China Ser. D-Earth. Sci.* 39 (8), 1046–5108. doi:10.1007/s11430-009-0111-2

Yang, S-Y., Jiang, S-Y., and Palmer, M. R. (2015). Chemical and boron isotopic compositions of tourmaline from the Nyalam leucogranites, South Tibetan Himalaya: Implication for their formation from B-rich melt to hydrothermal fluids. *Chemi.Geolo.* 419, 102–113. doi:10.1016/j.chemgeo.2015.10.026

Yavuz, F., Karakaya, N., Yıldırım, D. K., Karakaya, M. Ç., and Kumral, M. (2014). A Windows program for calculation and classification of tourmaline-supergroup (IMA-2011). *Compute.&eosciences* 63, 70–87. doi:10.1016/j.cageo.2013.10.012

Yin, A., and Harrison, T. M. (2000). Geologic evolution of the Himalayan-Tibetan orogen. *Annu. Rev. Earth Planet. Sci.* 28 (1), 211–820. doi:10.1146/annurev.earth.28.1.211

Yin, A. (2006). Cenozoic tectonic evolution of the Himalayan orogen as constrained by along-strike variation of structural geometry, exhumation history, and foreland sedimentation. *Earth-Science Revi.* 76 (1), 1–131. doi:10.1016/j.earscirev.2005.05.004

Yu, S-m., Ma, X-d., Hu, Y-c., Chen, W., Liu, Q-p., Song, Y., et al. (2021). Post-subdution evolution of the Northern Llasa Terrane, Tibet: Constraints from geochemical anomalies, chronology and petrogeochemistry. *China Geolo.* 5 (1), 84–95. doi:10.31035/cg2021045

Zhang, Y., Yin, C., Davis, D. W., Li, S., Qian, J., Zhang, J., et al. (2022). Mechanism of crustal thickening and exhumation of southern Lhasa terrane during the Late Cretaceous: Evidence from high-pressure metamorphic rocks of the Eastern Himalayan Syntaxis. *GSA Bulle.* doi:10.1130/b36366.1

Zhao, H-D., Zhao, K-D., Palmer, M. R., and Jiang, S-Y. (2019). *In-situ*elemental and boron isotopic variations of tourmaline from the Sanfang granite, South China: Insights into magmatic-hydrothermal evolution. *Chemi. Geolo.* 504, 190–204. doi:10.1016/j.chemgeo.2018.11.013

Zhao, H-D., Zhao, K-D., Palmer, M. R., Jiang, S-Y., and Chen, W. (2021a). Magmatic-Hydrothermal Mineralization Processes at the Yudong Ttn Deposit, South China: Insights from In Situ Chemical and Boron Isotope Changes of Tourmaline. *Econo. Geolo.* 116 (7), 1625–4167. doi:10.5382/econgeo.4868

Zhao, K-D., Zhang, L-H., Palmer, M. R., Jiang, S-Y., Xu, C., Zhao, H-D., et al. (2021b). Chemical and boron isotopic compositions of tourmaline at the Dachang Sn-polymetallic ore district in South China: Constraints on the origin and evolution of hydrothermal fluids. *Mine Depos.* 56, 1589–6108. doi:10.1007/s00126-021-01045-4

Zhao, Z-b., Li, C., and Ma, X-x. (2021c). How does the elevation changing response to crustal thickening process in the central Tibetan Plateau since 120 Ma?. *China Geolo.* 4 (1), 32–43. doi:10.31035/cg2021013

Zheng, B., and Chen, M. (2021). Gem Elbaite as a Recorder of Pigmatite Evolution: *In situ* Major, Trace Elements and Boron sotope Analysis of a Colour-Zoning Tourmaline Crystal. *Crystals* 11, 1363. doi:10.3390/cryst11111363

Zhou, Q., Wenchang, L., Wang, G., Liu, Z., Lai, Y., Huang, J., et al. (2019). Chemical and boron isotopic composition of tourmaline from the Conadong leucogranite-pegmatite system in South Tibet. *Lithos* 326-327, 529–359. doi:10.1016/j.lithos.2019.01.003